Lawrence Berkeley National Laboratory

Title

THE ROLE OF DEEP INELASTIC PROCESSES IN NUCLEAR PHYSICS: EXPERIMENTAL AND THEORETICAL ASPECTS OF DEEP INELASTIC REACTIONS

Permalink

Author

Moretto, L.G.

Publication Date

1979-03-01

Peer reviewed

THE ROLE OF DEEP INELASTIC PROCESSES
IN NUCLEAR PHYSICS:
EXPERIMENTAL AND THEORETICAL ASPECTS OF DEEP INELASTIC
REACTIONS

L. G. Moretto

Nuclear Science Division
Lawrence Berkeley Laboratory
University of California
Berkeley, California 94720

ABSTRACT

The collective modes excited in deep-inelastic reactions and
their natural hierarchy provided by their characteristic relaxation
times is described. The relaxation of the mass asymmetry mode is
discussed in terms of a diffusion process. Charge distributions and
angular distributions as a function of Z calculated with this model
are in good agreement with experimental data. This diffusion model
also treats the transfer of energy and angular momentum in terms of
particle transfer, and is successfully compared with experimental γ-ray
multiplicities as a function of both Q-value and mass asymmetry. The
angular momentum transfer is again considered in connection with the
sequential fission of heavy, deep-inelastic fragments and the excitation
of collective modes in the exit channel is considered. The role of the
giant El mode in the equilibration of the neutron-to-proton ratio is
discussed.

I.   INTRODUCTION

The spectacular evolution of a nucleus into two new nuclei as discovered in fission,[1] faced physicists with a large scale nuclear motion that was hardly matched by any well understood collective mode, and seemed to defy any attempt for a microscopic explanation. As the shell model and nuclear structure fluorished under a steady flow of spectroscopical data, nuclear fission for a long time remained a separate and stunted branch of nuclear physics. It was really a "vox clamantis in deserto" professing an altogether new perspective and phenomenology for nuclear physics.

Strutinski[2] showed how to calculate the potentia⊥ energy in collective space, but the fission process was to remain as mysterious as it was tantalizing. No matter how much one probed the compound nucleus, forming it with a variety of energies and angular momenta, not to speak of mass and charge, it would undergo fission, selecting its own collective paths in a way well beyond the view of the experimentalist.

What was clearly needed was a way to manipulate the initial conditions more or less precisely and yet flexibly to test the individual degrees of freedom under well defined conditions, possibly one by one. In fission this was never possible. At length, it occurred to the people of fission persuasion that heavy ions, possibly very heavy ions, provided the clue to the solution. The recipe: put together two nuclei with various kinetic energy, mass, charge, neutron-to-proton ratio, etc., and see what happens.

The spectacular phenomenology that has sprung forth is now well

documented in hundreds of papers and several review articles.[3-5] Its popularity has been confirmed (if it ever needed to be) by the large investments in heavy-ion facilities made by the international physics community.

Yet the traditional nuclear physics and the heavy ion phenomenology are not completely integrated. The language is still very different and, to some, the physics may appear almost unrelated. It may now be possible to dispel such worries. The phenomenological and macroscopic description of deep-inelastic processes reveals only the surface of a large body of microscopic features. But how do the microscopic degrees of freedom, so dear to nuclear structure, conspire to create the stupendous collective phenomena observed in heavy-ion reactions? This is the fundamental quest in heavy-ion studies and the essence of the many-body problem. It may also become the final and most ambitious goal in nuclear structure. At this point the title of this lecture becomes justified. The deep-inelastic process may well become, if it is not already, the most versatile workbench for the study of the many-body problem.

In what follows we want to briefly illustrate the salient features of deep-inelastic collisions and point out the most relevant microscopic implications. Rather than striving for completeness, we shall try to present those aspects which have particularly attracted the attention of our group both experimentally and theoretically. After a schematic description of the relevant degrees of freedom, we shall concentrate on attempts to understand the Z distributions and angular distributions as a function of Z in terms of a diffusion model. This approach will guide us towards the problem of angular momentum and energy transfer and

the one-body aspects of these processes. The problem of angular momentum transfer will be again considered in the study of sequential fission where the statistical excitation of collective modes in the exit channel will be suggested. Finally, we shall consider the effect of the giant El mode on the equilibrium neutron-to-proton ratio of deep-inelastic fragments.

II. DEGREES OF FREEDOM EXCITED IN DEEP-INELASTIC PROCESSES AND THEIR RELAXATION TIMES

Because heavy-ion reactions involve a broad range of interaction times, it is useful to associate a characteristic time with the evolution of each excited collective mode, namely the relaxation time. Estimates of these relaxation times provides a natural hierarchy for categorizing the various collective degrees of freedom. The exercise obtained in estimating these relaxation times is also very effective in acquainting one with the landscape provided by heavy-ion reactions. Let us first list the degrees of freedom and try to estimate the relaxation times. The most prominent modes to date include the relaxation of the

1) Relative motion

2) Neutron-to-proton ratio

3) Rotational degrees of freedom

4) Mass asymmetry.

a) The relaxation of the relative motion degree of freedom and the energy thermalization

Although a wide range of Q-values are observed in heavy-ion reactions, extending from zero to nearly complete relaxation, the strong energy damping is so prominent that it has led to the labelling of these

reactions as "deep-inelastic" processes. In several cases when the
ratio of the center-of-mass kinetic energy to the Coulomb barrier, E/B,
is larger than 1.5, interesting patterns[6] are seen in the cross section
plotted as contour lines in the total kinetic energy-angle plane (see
Fig. 1). The pattern can be related to the deflection function if one
can relate the energy loss with angular displacement from quasi-elastic
peaks. If one assumes that the system rotates with angular velocity

$$\omega = \frac{\ell_{ave}\hbar}{\mu r_o^2} \tag{1}$$

and that the centroid of the quasi-elastic peak decays exponentially
with time, one obtains a relaxation time given by

$$\tau_E = \frac{\theta_g - \theta}{\omega}\left[\ell n\left\{\frac{E(\theta_g) - E_o}{E(\theta) - E_o}\right\}\right]^{-1} \tag{2}$$

where θ_g is the grazing angle, θ is the angle of observation, and $E(\theta)$
is the centroid of the kinetic energy at that angle. For a typical system
one obtains $\tau_E \cong 3.0 \times 10^{-22}$ sec which is very short time indeed and is
barely larger than a nucleonic period. For E/B ratios smaller than 1.5,
the cross section patterns in the kinetic energy-angle plane are more
complex, and depend dramatically upon the mass asymmetry (Fig. 2).
However, the mean kinetic energies, for angles far removed from grazing
are well below the Coulomb energies of two touching spheres (Fig. 3).
One may question where the kinetic energy goes. It is remarkable that,
for the most part, the missing kinetic energy is found as fragment
excitation energy and the two fragments appear to be in thermal equilib-
rium.[7,8] Figure 4 shows some results obtained in our study[7] of the

reaction 340 MeV ^{40}Ar and ^{nat}Ag. The simultaneous detection of both fragments together with the measurement of both kinetic energies, both angles and the Z of one fragment enables one to reconstruct the average kinematics and deduce the pre-evaporation fragment masses as well as the mean number of neutrons emitted by each fragment. The results of such an analysis are consistent with an isothermal sharing of the excitation energy.

The thermalization of kinetic energy is substantial even at high bombarding energies. In an experiment, ^{63}Cu was bombarded with ^{20}Ne at 158, 252 and 343 MeV. The coincident fragments were identified in Z and their kinetic energy measured. The missing charge near symmetric splitting could then be determined as a function of total exit channel kinetic energy (Fig. 5a). The missing charge dramatically increases with bombarding energy, and depends linearly upon the excitation energy which can be estimated from kinematics (Fig. 5b). The slope of the line corresponds to about 25 MeV/charge. Since the total mass loss is about twice the evaporated charge, one obtains an average energy loss for particles of ~12.5 MeV, consistent with a simple estimate from evaporation. This indicates that even at the highest bombarding energies the near symmetric fragments are very close to complete thermalization. Recent results based upon the direct measurement of the emitted neutrons shows that this thermal equilibrium between fragments is established for a broad range of Q values.[9,10]

b) The neutron-to-proton ratio

When two nuclei having different neutron-to-proton ratios come in contact, it is expected that their neutron-to-proton ratio will change so that the potential energy of the two touching nuclei is minimized.

This has been seen in several instances.[11-13] Even more interesting is the observation (see Fig. 6) that for a given fragment Z the isotopic distribution changes as one moves in angle from the quasi-elastic to the deep-inelastic region.[3] In the quasi-elastic region the neutron-to-proton ratio is correlated with that of the projectile while in the relaxed region the ratio is more typical of the equilibrated system. Using the same method as above, one estimates a relaxation time of $\tau_{N/Z} \cong 1.3 \times 10^{-22}$ sec, even faster than the relaxation of the kinetic energy.

c) The rotational degrees of freedom

As two nuclei approach one another, the angular momentum is exclusively concentrated in orbital motion. During the interaction, the two nuclei can start spinning as angular momentum is transferred from orbital to intrinsic rotation. A secular equilibrium is reached when the angular velocities of the orbital and intrinsic motion are matched. At this point the system is said to be rotating rigidly. Rigid rotation implies a definite partition of angular momentum between orbital and intrinsic motion. Intrinsic angular momentum can be inferred from the γ-ray multiplicity associated with deep-inelastic collisions. In the reaction ^{nat}Ag + 175 MeV ^{20}Ne (see Fig. 7) the rigid rotation limit is attained at $\theta_{lab} \sim 90°$ while at more forward angles rigid rotation is not observed.[15] Assuming that the events at 90° correspond to trajectories which have orbited past 0°, one obtains an upper limit for the angular momentum relaxation time, $\tau_{\ell} = 15.0 \times 10^{-22}$ sec.

d) <u>The mass asymmetry</u>

A great variety[4,16] of mass or charge distributions have been observed in deep-inelastic reactions — from extremely narrow ones for ratios of $E/B < 1.5$, to very broad ones for ratios of $E/B > 1.5$ (see Fig. 8). As the interaction time increases, the particle exchange also increases, leading to mass or charge d.·tributions which are progressively broader. Even at fixed bombarding energy the breadth of the mass distribution is seen to vary with angle.[17] From the angular dependence of the mass distribution breadth one can infer the relaxation time: $\tau \cong 60 \times 10^{-22}$ sec, by far the largest observed so far. It is indeed the length of this relaxation time, slightly longer than the typical interaction times, that has allowed a detailed study of the equilibration of the mass asymmetry degree of freedom and has led to the formulation of diffusion models.

III. THE TIME EVOLUTION OF THE MASS ASYMMETRY MODE
   IN TERMS OF DIFFUSION THEORIES

The varied pattern of equilibrium and nonequilibrium features characteristic of heavy ion reactions prompted the suggestion that a diffusive regime should be prevailing at least for the slowest collective modes.[18-20] In other words, it was expected that a slow collective mode like the mass asymmetry would evolve in a Markovian fashion toward equilibrium by maintaining a strong coupling to the heat bath provided by all the other degrees of freedom. The applicability of the Master equation and of the Fokker Planck equation to the time evolution of the various collective modes has been discussed in detail without a clear-cut conclusion. However, the success of their application to a great variety

of features in heavy-ion reactions is undoubtable. Therefore, we shall try to illustrate some of their applications to the analysis of the Z distributions, angular distributions, and angular momentum transfer.

If we assume that the intermediate complex has a shape close to that of two touching fragments, the asymmetry of the system can be characterized by either the mass or the charge of one of the two fragments. We further assume that the time evolution along the asymmetry coordinate is diffusive in nature and describable in terms of the Master Equation:

$$\dot{\phi}(Z,t) = \int dZ' [\Lambda(Z,Z')\phi(Z',t) - \Lambda(Z',Z)\phi(Z,t)] \qquad (3)$$

where $\phi(Z,t)$ and $\dot{\phi}(Z,t)$ are the populations of the configurations characterized by the atomic number Z of one of the fragments and their time derivative at time t; and $\Lambda(Z,Z')$ and $\Lambda(Z',Z)$ are the macroscopic transition probabilities.

If in Eq. (3) one writes $Z' = Z+h$ and all the quantities are expanded about Z in powers of h, one obtains to low order:

$$\phi(Z,t) = -\frac{\partial}{\partial Z}[\mu_1\phi] + \frac{1}{2}\frac{\partial^2}{\partial Z^2}[\mu_2\phi] \qquad (4)$$

which is the well-known Fokker-Planck equation. The quantities μ_1 and μ_2 in Eq. (4) are the first and second moment of the transition probabilities

$$\mu_1 = \int h\Lambda(Z,h)dh ; \qquad \mu_2 = \int h^2\Lambda(Z,h)dh . \qquad (5)$$

The Fokker-Planck equation has simple analytical solutions when μ_1, μ_2 are constants and for the initial condition $\phi(Z,0) = \delta(Z-Z_0)$:

$$\phi(Z,t) = (2\pi\mu_2 t)^{-\frac{1}{2}} \exp\left\{-[Z - (Z_0 + \mu_1 t)]^2/2\mu_2 t\right\} . \qquad (6)$$

Notice that the centroid of the Gaussian moves with velocity μ_1 which can be related to the driving force $F = -V_Z'$ and to the friction coefficient K by the relation: $K = \mu_1 F$.

When the force is harmonic,

$$V_Z = \frac{c}{2}(Z - Z_{sym})^2 = \tfrac{1}{2}ch^2 \quad ,$$

an analytic solution is also available

$$\phi(h,t) = c^{\tfrac{1}{2}}\left[2\pi T\left(1 - \exp - \frac{2ct}{K}\right)\right]^{-\tfrac{1}{2}} \times \exp\left\{-\frac{c[h - h_0 \exp - ct/K]}{2T(1 - \exp - 2ct/K)}\right\}$$

(7)

where we have made use of the Einstein relation $\mu_1/\mu_2 = -V_Z'/2T$ and T is the temperature. From general phase space considerations one can consider the following ansatz for the transition probabilities.[19]

$$\Lambda(Z,Z') = \lambda(Z,Z')\rho_Z = \frac{\kappa f \rho_Z}{(\rho_Z \rho_{Z'})^{\tfrac{1}{2}}}$$

where $\lambda(Z,Z')$ is the microscopic transition probability, ρ_Z is the final state density, κ is a particle flux, and f is the window area between the two fragments. This can be rewritten as

$$\Lambda(Z,h) = \kappa f \exp(-V_Z' h/2T) \quad . \tag{8}$$

The Fokker-Planck coefficients can then be calculated as

$$\mu_1 = -2\kappa f \sinh V_Z'/2T \approx -\frac{\kappa f V_Z'}{T} \quad ,$$

$$\mu_2 = 2\kappa f \cosh V_Z'/2T \approx 2\kappa f \quad , \tag{9}$$

which for large T satisfies the Einstein relation. Such an ansatz

implies for the friction coefficient: $K = T/\kappa f$.

In Eq. (9), the quantity κf can be considered a form factor for the transition probability, which should depend upon the overlap between the two fragments. If one takes the idea of a particle transfer seriously, it is possible to write such a quantity, which is a particle transfer rate, as suggested by Randrup[21]

$$\kappa f \;\hat{=}\; \int n d\sigma \;=\; 2\pi n_o \bar{R} b \; \psi(\zeta) \tag{10}$$

where n_o is the particle flux in nuclear matter at saturation density, $R = C_1 C_2/(C_1 + C_2)$ is a reduced radius expressed in terms of the central radii of the two fragments, b is the skin thickness, and $\psi(\zeta)$ is a universal function depending upon the separation between the sharp surface of the two fragments in units of the surface thickness. This approach neatly factors out the geometrical features of the problem.

In general, the potential energy of the intermediate complex as a function of Z can be written as

$$V(Z,\ell) \;=\; V_{LD}(Z) + V_{LD}(Z_T - Z) + V_{prox}(Z, \ell) + V_{Coul} + V_{rot} \tag{11}$$

where ℓ is the total angular momentum, V_{LD} represents the liquid drop energies of the two fragments, and V_{prox} is the nuclear interaction or proximity energy.[22]

The total potential V depends on the fissionability of the system x, on ℓ and on the distance between centers D. At low values of all these parameters, V monotonically increases from $Z=0$ to Z_{sym} where it reaches a maximum. As x, ℓ, and D increase, the second derivative at Z_{sym} goes through zero and changes sign; thus for large

values of these parameters, V initially increases with Z, it reaches a maximum at some intermediate value of Z, it then decreases until it reaches a minimum at Z_{sym}.

The driving force which arises from this potential depends dramatically on the entrance channel asymmetry, as well as on x, ℓ, D. It may either drive the system towards symmetry or towards extreme asymmetries. For a reaction like 620 MeV Kr + Au, the driving force is in the direction of symmetry most of the time.[17] The potential energies for such a system are plotted in Fig. 9 as a function of the Z of one of the fragments for various angular momenta. The Master Equation can be solved to obtain the probability distribution along the main asymmetry coordinate as a function of time. The results of such a calculation can be seen in Fig. 10 for the potential energies shown in Fig. 9. The one-body friction has been used with moderate success to evaluate the dynamical aspects of the reaction. From it an average interaction time can be obtained as well as an average window to be used in the diffusion calculation. With these quantities one can then solve either the Fokker-Planck or the Master Equation to obtain the charge and angular distributions. The results of a calculation[23] of the latter type for the reaction ^{197}Au and ^{181}Ta + ^{86}Kr are shown in Fig. 11 and 12. It is rewarding to notice that not only are the Z distributions reproduced with remarkable accuracy, but also the angular distributions associated with individual asymmetries. The latter fit is perhaps the most demanding of the theory. It can be obtained only if the ℓ dependence of the interaction times and of the diffusion coefficient are accurately predicted. Any theory will find it relatively easy to fit the Z distribution but will have to prove its soundness in fitting the angular distribution as a function of Z.

IV.   THE RELAXATION OF ROTATIONAL DEGREES OF FREEDOM

Encouraged by this success we can try to study a problem which is intimately related, namely the dependence of the angular momentum transfer upon Q value and mass asymmetry.[24]   The total kinetic energy can be written as

$$E = V_{Coul}(Z) + \frac{\hbar^2 \ell^2_{rel}(Z,\ell)}{2\mu(Z)\ d^2(Z)} \tag{12a}$$

where ℓ_{rel} is the orbital angular momentum in the exit channel, μ is the reduced mass, d is the distance of the two fragments at scission, and Z is the atomic number of one of the two fragments.   It follows that the above problem is equivalent to drawing the lines of constant entrance channel angular momentum in the plane of the total kinetic energy and of the fragment atomic number.   Empirical precriptions suggesting that such lines are horizontal lines parallel to the Z axis[25] appear so dangerous that a deeper study is warranted.

In the limit of infinite radial friction (the relevance of which is discussed in a later section of this lecture), there are two limiting patterns these lines should display, corresponding to the two extreme regimes associated with the rotational degrees of freedom of the intermediate complex.   In the first limiting case the reaction occurs with no transfer of angular momentum from orbital motion to intrinsic spin. In this case, the angular momentum of relative motion as a function of Z, $\ell_{rel}(Z,\ell)$ is a constant independent of Z and equal to ℓ.   The curves in Fig. 13a show examples for this case assuming the shape of the complex to be two touching spheres.

In the second limiting case the complex is rotating as a rigid body at the time of scission, regardless of the impact parameter (ℓ-wave). In this case, the relative angular momentum is Z-dependent, and given by

$$\ell_{rel}(Z,\ell) = \frac{\mu_Z \, d_Z^2}{\mu_Z d_Z^2 + I(Z) + I(Z_T-Z)} \cdot \ell \qquad (12b)$$

where $I(Z)$ is the moment of inertia of a fragment with charge Z about its own axis, and Z_T is the total charge in the composite system. This expression can be substituted in Eq. (12a) to calculate the lines of constant ℓ for this case. The curves in Fig. 13b show examples of this behavior for the same ℓ-waves as for the previous case.

These two cases may be considered as the regimes prevailing at short and long interaction times, respectively. For short interaction times, as in nearly grazing trajectories, the first mechanism is expected to be relevant for Z's close to the projectile. If angular momentum transfer (from orbital to intrinsic spin) is mediated by nucleon exchange between the reaction partners, the amount of ℓ-transfer must be a function of the number of nucleon exchanges, which is directly related to the interaction time. Even though the average lifetime of the complex may be short, the fragments with Z's far removed from the projectile are associated with systems which have survived the longest. Thus, one would expect the ℓ-transfer for that particle asymmetry to be very large. Qualitatively, one would expect the correct curve for near grazing ℓ-waves to look like the dotted curve in Fig. 13c. For ℓ-waves associated with longer interaction times, one would expect the ℓ-transfer to be almost complete, even for Z's near the projectile, since many nuclear exchanges will have occurred during the time of interaction,

although the net exchange may be small. Therefore, one would expect

the curves to look like those in Fig. 13b. A more reliable conclusion

on the qualitative and quantitative aspects of this problem can be

obtained from a model calculation.

Consistent with experiment, it is assumed that the radial

kinetic energy is dissipated immediately at the interaction radius.

(For the lowest ℓ-waves, the interaction times appear to be long compared

to the relaxation time of the radial kinetic energy, and for the highest

ℓ-waves, even though the interaction times are short, very little of the

kinetic energy is in the radial coordinate). The analysis is restricted

to a system of two spheres separated by an ℓ-dependent distance, $d(\ell)$,

dynamically determined as described further on in the text. We need to

calculate how the orbital angular momentum (ℓ_{rel}) is transferred into

the spins of the nuclei (I_1, I_2) and the functional dependence of I_1

and I_2 on the asymmetry of the complex (Z). This calculation may be performed in two steps:

1) The complex, initially at asymmetry Z_p, is assumed to live at time t and to decay with asymmetry Z. The average rate of change of the charge of nucleus 1 is $\dot{Z}_1 = (Z-Z_p)/t$. Since the charge-to-mass ratio has been shown experimentally to equilibrate on a much faster time scale than the charge-asymmetry mode, one may write

$$\dot{A}_1 = (Z - Z_p)\alpha /t \tag{13}$$

where A_1 is the mass of nucleus 1 and α is the A/Z ratio for the composite system. The average rate of nucleon transfer from one nucleus to the other is given by $n_0\sigma$, where n_0 is the bulk flux of nuclear matter and σ is the effective window between the nuclei. By forcing the system to arrive at asymmetry Z at time t, we impose an asymmetry on the right (r_{12}) and left (r_{21}) nucleon transfer rates, which can be written as

$$r_{12} = n_0 - \tfrac{1}{2}\dot{A}_1 \quad ,$$
$$r_{21} = n_0 + \tfrac{1}{2}\dot{A}_1 \quad . \tag{14}$$

Knowing these transfer rates, we can write the following system of coupled differential equations for the spins and the orbital angular momenta:

$$\dot{I}_1 = d_1\left[r_{12}d_1(\dot{\theta} - \dot{\theta}_1) + r_{21}d_2(\dot{\theta} - \dot{\theta}_2)\right] / \hbar$$

$$\dot{I}_2 = d_2\left[r_{12}d_1(\dot{\theta} - \dot{\theta}_1) + r_{21}d_2(\dot{\theta} - \dot{\theta}_2)\right] / \hbar \tag{15}$$

$$\dot{\ell}_{rel} = -(\dot{\ell}_1 + \dot{\ell}_2)$$

where d_1 and d_2 are the distances of the nuclear centers from the window

and $\dot{\theta}$, $\dot{\theta}_1$, $\dot{\theta}_2$ are the rotational frequencies for the orbital motion, spin 1 and spin 2, respectively. By integrating Eqs. (15) and (13), subject to the proper initial conditions, we arrive at values for $I_1(Z,\ell,t)$ and $I_2(Z,\ell,t)$.

2) The functions $I_1(Z,\ell)$, $I_2(Z,\ell)$ are obtained by integrating out the time dependence. The average lifetime of the complex for a given ℓ-wave is approximated as the time necessary for the dynamical system with no mass transfer to return to the strong absorption radius under the influence of the Coulomb and the Proximity potentials and subject to Proximity friction. A Gaussian lifetime distribution, $\pi(t,\ell)$, about this average value is used with a variance given by $\sigma^2(\ell) = 1.5 \, \tau(\ell)$. The quantity $d(\ell)$ [mentioned earlier] is the average value of the distance between centers along the trajectory using the Proximity Flux function $\psi(r)$ for the probability weight function. It is also necessary to weight the $I_i(Z,\ell,t)$ by the probability for forming the system Z at time t. This function, $\phi(Z,t)$, can be obtained by solving a Master Equation or an associated Fokker-Planck equation.

Figure 14a shows the predictions of the model of the system 1156 MeV ^{136}Xe + ^{197}Au. Each pair of adjacent lines brackets 5% of the reaction cross section. The qualitative behavior predicted above is now very apparent. Figure 14b shows the upper portion of Fig. 14a with contours of constant cross section (as calculated by the Fokker-Planck equation) drawn in. The horizontal lines divide the data into ten bins, 30 MeV wide. (Only every other line is shown for ease of viewing.) The lines of constant ℓ calculated by the model are chosen to coincide with the parallel lines at the Z of the projectile. Figure 15 is a plot of the ratio of the variance predicted by the present model and the variance

derived from the parallel cuts. Note the large difference for the first few bins. It is exactly in this energy region that a previously mentioned discrepancy between the experimental and theoretical (one-body theory) energy loss per particle was found. The empirical analyses seemed to indicate that the experimental energy loss per particle, calculated as

$$\varepsilon = \frac{(E_{cm} - TKE_{bin})}{[\sigma_Z^2 \cdot \alpha]} \tag{16}$$

was between two and three times larger than that expected from a one-body dissipation mechanism. If the empirical variances are in error by as much as indicated by the present work, the discrepancy between theory and experiment disappears.

This model, which allows one to calculate the Z and Q value dependence of the intrinsic angular momentum, can be used to analyze the experimental γ-ray multiplicities.[26,27] All that is needed is a transformation from angular momentum to γ-ray multiplicity. The transformation from fragment spin to γ-ray multiplicity is based upon the assumption that most of the fragment angular momentum is removed by stretched E2 decay. More specifically we use the following transformation:

$$\langle I_1(Z_1 E_k) \rangle + \langle I_2(Z_1 E_k) \rangle = 2(M_\gamma - 2a) \tag{17}$$

where I_1 and I_2 are the fragment spins, M_γ is the γ-ray multiplicity, and a is the mean number of statistical γ-rays emitted by each fragment. Compound nucleus studies with heavy-ion reactions indicate that $a \cong 2 - 3.5$ depending upon the nucleus.[28] Because of this uncertainty, caution must be exercised in comparing the absolute values of the measured and calculated multiplicities.

The kinetic energy dependence of the γ-ray multiplicities will be considered first. In Fig. 16 the γ-ray multiplicity M_γ associated with both fragments in the reactions Au, Ho, Ag + 618 MeV ^{86}Kr is plotted as a function of the total kinetic energy of each pair. Both in the experiment and in the theory, the γ-ray multiplicities are integrated over all the exit channel asymmetries. The number of statistical γ-rays per fragment is taken to be three.

The plateau in the experimental multiplicities and the maximum in the calculated multiplicities corresponds to a regime very close to rigid rotation. The theoretical drop at lower kinetic energies is due to the effect of the Coulomb energy (which in the model is taken to be that of two touching spheres) and the fact that lower angular momenta, in the limit of rigidly rotating touching spheres, are associated with lower kinetic energies. The experiment does not show a drop in multiplicity as large as the theory does because the exit channel configuration is not constrained to that of two touching spheres. Thus the deep-inelastic component is spread over an energy range extending well below the Coulomb barrier. Furthermore, fluctuations in shape may destroy the simple correlation between kinetic energy and angular momentum predicted by the model at these low energies.

The second aspect to be analyzed is the Z-dependence of M_γ in the quasi-elastic region. Examples of data are shown in Fig. 7 and 17. Calculations for some of these cases are shown in Fig. 19. The characteristic V-shaped pattern is very nicely reproduced by the calculations. The qualitative explanation of this pattern is again rather simple. Fragments close in Z to the projectile and with substantial kinetic

energy on the average have exchanged fewer nucleons than fragments farther removed in Z from the projectile. Thus less angular momentum is transferred to the former than to the latter fragments, giving rise to the rapid increase of the γ-ray multiplicity as one moves away from the projectile in either direction. This good agreement is consistent with the agreement observed between experiment and theory in Fig. 16 at the highest kinetic energies. From both of these figures one is tempted to conclude that particle exchange is sufficient to quantitatively explain the dependence of the angular momentum transfer upon kinetic energy loss, without invoking the excitation of giant collective modes. Apparently the same one-body theory that reproduces both the Z distributions and the angular distributions versus Z so satisfactorily, also handles the energy and angular momentum transfer more than adequately.

The final aspect to be considered is the Z dependence of the γ-ray multiplicity in the deep-inelastic region. Examples of data are shown in Fig. 18 and of calculations are given in Fig. 19. Again, the experimental data are reproduced quite well. It must be emphasized that in this energy region the calculation predicts near rigid rotation throughout the Z range. Yet the rise of M_γ with decreasing Z, commonly considered a fingerprint of rigid rotation is conspicuously absent. The reason for this behavior is to be found in the angular momentum fractionation along the mass asymmetry coordinate as first inferred elsewhere.[26] The main cause for angular momentum fractionation is the interaction time dependence upon ℓ. The high ℓ-waves are characterized by a short interaction time and cannot spread too far away from the entrance channel asymmetry. The low ℓ-waves are characterized by a longer interaction

time and can populate asymmetries farther removed from the entrance channel. Consequently as one moves towards more extreme asymmetries one selects progressively lower ℓ-waves.

Furthermore, at high angular momentum, the driving force is strongly directed towards the higher Z's and discourages any diffusion towards low Z's (see Fig. 9). As the angular momentum decreases, the driving force also diminishes and may even reverse its direction, thus allowing for a substantial diffusion to occur in the direction of the low Z's. Consequently the low Z's are selectively populated by low ℓ-waves and hence the lack of rise in the γ-ray multiplicity with decreasing Z.

V.   SEQUENTIAL FISSION AND THE EXCITATION OF COLLECTIVE
MODE IN THE EXIT CHANNEL OF DEEP-INELASTIC REACTIONS

An interesting phenomenon, accompanying the deep-inelastic process, namely the fission of the heavy partner, has recently been observed[30] in the reaction ^{197}Au + 979 MeV ^{136}Xe. This special kind of decay can potentially provide information on:

a) the transfer of angular momentum from orbital to intrinsic
    rotation

b) the transfer of energy from the entrance channel to internal
    degrees of freedom

c) the possibility of prompt fission of the heavy partner in
    the Coulomb and nuclear fields of the light fragment.

Recently[31] we have studied sequential fission in the reaction ^{197}Au + 620 MeV ^{86}Kr with an apparatus consisting of a ΔE(gas), E(solid state) telescope to identify the atomic number Z_3 and energy E_3 of the light

partner, and a large, solid angle, X-Y position-sensitive counter to simultaneously detect either the heavy partner (Z_4) or one of its fission fragments. The latter detector,[32] which has a position resolution of 1°, and subtends 24° both radially and vertically, provides information on both the energy E_4 and the in- and out-of-plane angular distributions of the correlated fragments.

Figure 20a depicts cross section contour lines in the E_4-Z_3 plane and illustrates the clear separation between the non-fissioning binary events and the sequential fission events. To obtain the fission probability of the heavy fragment (Z_4), the number of singles events for the corresponding Z_3 value were compared with the number of coincidence, non-fission events (after correction for the coincidence efficiency which was measured with elastic scattering). In Fig. 20b, this fission probability, integrated over the deep-inelastic region of E_3, is shown as a function of Z_3. Although the fission probability is quite small, around $Z_3=40$ ($Z_4=75$), it rises very rapidly and approaches 100% for $Z_3 < 30$ ($Z_4 > 75$).

In Fig. 21 the fission probabilities for the heavy recoils are shown as a function of the light fragment kinetic energy for representative atomic numbers. For all cases the fission probability increases with decreasing kinetic energy E_3. Qualitatively, these features can be understood in terms of a fission barrier which decreases with increasing Z_4 and an excitation energy E_4^* which increases with decreasing E_3. These fission probabilities reach astoundingly large values at the highest excitation energies, namely > 80% even for recoils with an atomic number of 79. Because of partial wave distribution in heavy-ion reactions,

fission may select out the very highest angular momentum transfers which enhances the fission probability. Thus the ℓ-distribution of the sequential fission channel may not at all reflect the overall ℓ-distribusion for the deep-inelastic process as a whole.

The out-of-plane angular distributions of the fragments from sequential fission are nearly Gaussian and are peaked on the reaction plane. The FWHM of these distributions in the laboratory and in the c.m. of the recoiling heavy fragment are shown as a function of Z_3 in Fig. 22. For fission fragments originating from elements heavier than the target ($Z_3 < 36$) the c.m. width is $47°-50°$, in agreement with the previously measured value,[33] which is an average over the entire Z-distribution. One should note that the out-of-plane angular distribution for a binary reaction not followed by fission (see Fig. 22) appears to be consistent with the de-excitation of both fragments mainly by neutron emission.

The out-of-plane angular distribution of fission fragments may be due to two possible causes (which are not mutually exclusive): 1) the fluctuations of the fission axis about the normal to the angular momentum; and 2) the misalignment of the primary fragment angular momentum. If the angular momentum of the primary fragments is aligned ($M = J$), the emitted gamma rays, which are expected to be mostly stretched E2 decays, should show a strong anisotropy, though attenuated by the presence of E1 decays. The expressions for the angular distributions arising from completely aligned systems are[34]

$$\text{E2: } W(\theta) = (5/4)(1 - \cos^4\theta) \text{ , } \quad \text{E1 : } W(\theta) = (3/4)(1 + \cos^2\theta)$$

where θ is the angle of emission with respect to the angular momentum direction. However, the evidence[35,36] is that the gamma ray angular

distribution is <u>isotropic</u> to within 5-35%. This fact can, to some extent, be explained away by invoking E1 decay. However, a very unlikely 50-50 contribution from E1 and E2 is barely sufficient to explain the largest measured anisotropy of 1.35. This dilemma forces one to either abandon the assumption of stretched E2 decays, which is disastrous because it compromises all our understanding of the yrast decay, or to seek another explanation. Recently, Berlanger et al[35] proposed that bending vibrations could be excited in the primary deep-inelastic process. Along the same line, but more generally, we suggest that collective modes like bending (doubly degenerate) and twisting (non-degenerate) may be thermally excited thus generating <u>random</u> components in the angular momentum.

If we assume such a depolarization mechanism, simple statistical considerations lead to the following partition function (for simplicity an intermediate complex consisting of two equal touching spheres is assumed)

$$Z = (4\pi)^2 \int I^2 \exp(-I^2 / \mathcal{J} T) \, dI \tag{18}$$

and

$$\ln Z = a + 3/2 \ln(\mathcal{J} T) \tag{19}$$

where $\mathcal{J}$ is the moment of inertia of one fragment, T is the temperature, and a is a constant. The resulting rms angular momentum per fragment is:

$$\overline{I^2} = -\frac{\partial \ln Z}{\partial [1/\mathcal{J} T]} = \frac{3}{2} \mathcal{J} T \quad . \tag{20}$$

For the present reaction of 618 MeV ^{86}Kr + ^{197}Au and using r_o = 1.22 fm and T = 2-3 MeV, $(\overline{I^2})^{\frac{1}{2}}$ is estimated to be about 13 to 16 $\hbar$ per fragment, randomly oriented, rather than perpendicular to the recoil direction.

(These results are not very sensitive to small deviations from symmetric splitting.)

By randomly coupling this angular momentum to that transferred from orbital motion (~30 $\hbar$ as is inferred from gamma-ray multiplicity data[26]) one obtains a rms angular momentum misalignment Φ' of the order of 24° to 28°, more than adequate to explain by itself the width of the out-of-plane sequential fission distribution. This misalignment comes from the deep-inelastic process itself. If this is the case, the explanation of the fission fragment out-of-plane distribution lies in a depolarization inherent to the deep-inelastic process and not in the fission mechanism. This explanation does not contradict the existence of fluctuations in the fission direction. However, one should note that the $(\overline{I^2})^{\frac{1}{2}}$ generated by these bending and twisting modes may be larger than K_0 and thus may be the dominant effect in producing the out-of-plane fission widths. The presence of such a depolarization substantially helps to explain the gamma-ray anisotropy with a much smaller amount of E1 transitions.

VI. THE GIANT E1 MODE AND ITS ENERGY BROADENING FROM
     THE CHARGE DISTRIBUTIONS IN HEAVY-ION REACTIONS

The giant E1 mode is best known through its photoexcitation which is manifested in a peak at an energy $E = 78 A^{-1/3}$ MeV with a width of typically 4-6 MeV. The same degree of freedom is involved in the charge distribution at fixed mass asymmetry in binary heavy-ion reactions[37] (and in fission). Since the equilibration of the E1 mode in heavy-ion reactions, or the equilibration of the neutron-to-proton ratio of the two fragments, seems to occur quickly, the most probable charges can be

obtained by minimizing the potential energy of the two fragments in contact with respect to the charge of one of the fragments at constant fragment mass. This well documented feature of heavy-ion reactions only provides information about the potential energy term of the collective E1 Hamiltonian. In principle one could obtain information for the whole Hamiltonian by a measurement of the charge distribution at fixed mass.

Since in the great majority of cases the E1 phonon energy is expected to be much larger than the temperature, the E1 mode is expected to be in its ground state. As an example, let us consider the reaction Ni + Ar at 280 MeV bombarding energy whose mass and charge distributions have been studied in detail.[11] From the maximum linear dimension of the intermediate complex one obtains the relevant E1 phonon energy: $\hbar\omega = 94/d = 8\text{-}10$ MeV, where d is the semi-major axis of the intermediate complex. From the internal excitation energy of the complex one obtains $T = \sqrt{E_x/a} = 2$ MeV. Since $\hbar\omega/T \cong 4\text{-}5 \gg 1$, the collective E1 mode should be mainly in its ground state. Therefore the Z distribution at fixed mass asymmetry should be given by the modulus square of the ground state wave function and the second moment of the distribution is expected to be

$$\sigma_z^2 = \frac{\hbar\omega}{2c} \cong 0.6\text{-}0.8 \ (\text{charge units})^2$$

where c is the stiffness constant associated with the E1 mode, or

$$V_{(E1)} = \frac{c(z - z_0)^2}{2} \ .$$

The analysis of the experimental charge and mass distribution shows that

mass and charge are strongly correlated as expected, with a correlation coefficient r = 0.97. However, the intriguing result for the second moment of the Z distribution at constant A is σ_Z^2 = 0.3 (charge units)^2, substantially smaller than expected. The disagreement is all the more evident since the experimental σ_Z^2 should be (and has not been) corrected for particle evaporation, which could decrease its value by an additional amount. Even more surprising is the fact that the experimental value of σ_Z^2 is well reproduced if one assumes just a classical statistical distribution in Z, namely,

$$\sigma_Z^2 = T/c \cong 0.3 \text{ (charge units)}^2$$

The outstanding problem is then to understand why the distribution in Z is classical rather than quantal, as one would expect.

The explanation may reside in the damping of the collective E1 mode. In photoexcitation, the giant resonance is mainly a 1p,1h state and presumably owes its width to the coupling into the 2p,2h states. In the present case, at relatively high excitation energy (60 MeV), the collective mode is an (np,nh) state which may couple into (n+1p, n+1h) or (np,nh), or again, ((n-1)p,(n-1)h) states. The resulting damping is energy-dependent and due mainly to the increasing density of the doorway states with increasing energy. It is interesting to see the consequence of this coupling to the Z distribution. Following Bohr and Mottelson[38] with a simple generalization, we can describe the coupling of the collective state |a⟩ to the doorway states |α⟩. The exact state |i⟩ is given by

$$|i\rangle = |a\rangle + \frac{P}{E_i - H_0 - V} V|a\rangle \qquad (21)$$

where $P = \sum_{\alpha} |\alpha\rangle \langle\alpha|$, H_0 is the unperturbed Hamiltonian, and V is the perturbation.

The relevant charge distribution is given by $p_i(z) = \int dx |\psi_i(z,x)|^2$, where $\psi_i(z,x) = \langle z,x|i\rangle$, and x denotes all other variables which must be projected out. In order to compare theory with experiment we have to consider the average of the distribution over an energy interval around E_i. We can write

$$p_i(z)_{ave} = \int dx \left[|\{\psi_i(z,x)\}_{ave}|^2 + \{|\psi_i^{fl}(z,x)|^2\}_{ave} \right]$$

(22)

with $\psi_i^{fl} = \psi_i - \{\psi_i\}_{ave}$ the "fluctuating" wave function. The fluctuating part can be shown to be responsible for the broadening of the distribution. It leads to a statistical distribution for Z. We want to show that the first term can lead to a narrowing of the distribution. For this purpose we have to consider the averaged Green function $\{1/(E_i-H_0-V)\}_{ave}$. This average has been considered extensively in the literature.[39] For large systems and high excitation energies only the average diagonal matrix elements of the resolvent have to be considered and it can be shown that

$$\left\{ \langle\alpha| \frac{P}{E_i-H_0-V} |\alpha\rangle \right\}_{ave} = \frac{1}{E_i - E_\alpha - i\Gamma}$$

(23)

where Γ is the imaginary part of the "equivalent optical potential" describing the dissipation of the state $|a\rangle$ into the states $|\alpha\rangle$. The amplitude of the state $|a\rangle$ contained in the average eigenstate $|i\rangle$ is given by

$$c_a(i) = \left(1 + \sum \frac{V_{\alpha a}^2}{(E_i - E_\alpha - i\Gamma)^2}\right)^{-\frac{1}{2}}, \quad (24)$$

D being the spacing of the states α.

In summary, and omitting for simplicity the bracket of the average,

$$|i\rangle = c_a(i)|a\rangle + \sum_\alpha c_\alpha(i)|\alpha\rangle \quad . \quad (25)$$

The next step is to establish that the sum over α is the above equation is a coherent one and thus the corresponding term describes a wave packet, i.e., it leads to a narrowing of the distribution. One can prove that if $V_{a\alpha}$ is random, the vectors $|\alpha\rangle$ contain phases which destroy the random property of $V_{a\alpha}$. Having established this point from first principles, we are entitled to use as first guess a simple-as-possible model. The average wave function associated with the charge asymmetry coordinate can be written as

$$\phi_i(z) = c_a(i)\psi_a(z) + \frac{1}{D}\oint dE_\alpha \, c_\alpha(i)\,\psi_\alpha(z) \quad (26)$$

where D is the level spacing of the available doorway states and $\psi_a(z)$ is the groundstate wave function of the El mode: $\psi_a(z) = \sqrt{2\pi\hbar\omega/c}$ $\exp[-cz^2/2\hbar\omega]$. Qualitatively one sees already that, as the coupling increases, the integral in Eq. (26) becomes progressively dominant and the more $|\alpha\rangle$ states that are called into play by the strength of the coupling, the narrower $\phi_i(z)$ becomes. As a qualitative first guess on the $\psi_\alpha(z)$ we can use the plane wave expression

$$\psi_\alpha(z) = \sqrt{2\pi\hbar\omega/c} \, \exp\left(iz\sqrt{c/2\hbar\omega}\sqrt{E\alpha/D_1}\right)$$

$$(27)$$

where the plane waves are normalized to unity in a z box of volume corresponding to that of the harmonic oscillator. By taking $\Gamma = \hbar(\lambda^+ + \lambda^0 + \lambda^-)$, where $\lambda^+, \lambda^0, \lambda^-$ are the transition probabilities from (np,nh) to (n+1p, n+1h), (np,nh) and (n-1p, n-1h) states, respectively,[37] the integral in Eq. (26) can be evaluated and gives as a result

$$2\pi \exp\left(-iz \sqrt{c/2\hbar\omega} \ \sqrt{1/D_1} \ \sqrt{E_i - i\Gamma}\right). \tag{28}$$

The second moment of the z distribution, σ_z^2, can then be obtained from the z distributions given by the modulus square of Eq. (26).

The calculated second moment of the distribution σ_z^2 versus excitation energy is shown in Fig. 23. The narrowing of the distribution with increasing energy is quite evident. Since this calculation does not include thermal fluctuations, they are introduced in the simplest way,

$$\sigma_z^2 = \sigma_{z,Q}^2 + \sigma_{z,T}^2 \tag{29}$$

where the labels Q and T stand for quantal and thermal. The possibility of experimentally observing the minimum of σ_z^2 and its rapid rise with decreasing energy is of extreme interest because it would provide us with information on the damping of a giant resonance in a hot nucleus. This is particularly attractive considering the extremely difficult alternatives, like gamma decay from highly excited nuclei.

V. CONCLUSION

In summary, the general features of deep-inelastic reactions have
been discussed emphasizing the mass asymmetry mode, the relative motion,
the transfer of angular momentum and the equilibration of the neutron-
to-proton degree of freedom. For the mass asymmetry mode, good agreement
has been observed between the experimental data and a diffusion model.
In addition, a natural extension of this model to include the transfer
of energy and of angular momentum via a particle transfer mechanism
has been discussed and successfully compared with experiment. The
agreement with gamma-multiplicity data not only supports the underlying
features of the diffusion model, but also lends credence to the one-body
nature of the energy and angular momentum transport processes. Further-
more, on the basis of sequential fission data it has been suggested
that the angular momentum transferred in deep-inelastic reactions may
be partially depolarized through the excitation of collective modes at
scission. This mechanism also explains the absence of an appreciable
gamma-ray anisotropy. Finally, the effect of the giant E1 mode on
the equilibrium neutron-to-proton ratio of deep-inelastic fragments
has been described. It has been shown that the widths of the Z distri-
butions for fixed mass asymmetry can be explained by the coupling of the
E1 mode to the intrinsic degrees of freedom.

REFERENCES

1. O.Hahn and F.Strassman, Naturwissenschaften **26**, 755 (1938).

2. V.M.Strutinsky, Nucl. Phys. **A95**, 420 (1967).

3. J.Galin, J. de Phys. **37**, C5-83 (1976) and references therein.

4. L.G.Moretto and R.Schmitt, J. de Phys. **37**, C5-109 (1976) and references therein.

5. W.U.Schröder and J.R.Huizenga, Ann. Rev. Nucl. Sci. **27**, 465 (1977) and references therein.

6. J.Wilczynski, Phys. Letters **47B**, 484 (1973).

7. B.Cauvin, R.Jared, P.Russo, R.P.Schmitt, R.Babinet, and L.G.Moretto, Nucl. Phys. **A301**, 511 (1977).

8. R.Babinet, B.Cauvin, J.Girard, H.Nifenecker, B.Gatty, D.Guerreau, M.Lefort, and X.Tarrago, Nucl. Phys. **A296**, 160 (1978).

9. B.Tamain, private communication.

10. A.Gavron, private communication.

11. B.Gatty, D.Guerreau, M.Lefort, X.Tarrago, J.Galin, B.Cauvin, J.Girard, and H.Nifenecker, Nucl. Phys. **A253**, 511 (1975).

12. B.Gatty, D.Guerreau, M.Lefort, J.Pouthas, X.Tarrago, J.Galin, B.Cauvin, J.Girard, and H.Nifenecker, Z. Phys. **A273**, 65 (1975).

13. J.C.Jacmart, P.Colombani, H.Doubre, N.Frascaria, N.Poffé, M.Riou, J.C.Roynette, C.Stéphan, and A.Weidinger, Nucl. Phys. **A242**, 175 (1975).

14. J.Barrette, P.Braun-Munzinger, C.K.Gelbke, H.L.Harney, H.E.Wegner, B.Zeidman, K.D.Hildenbrand, and U.Lynen, Nucl. Phys. **A299**, 147 (1978).

15. P.Glässel, R.S.Simon, R.M.Diamond, R.C.Jared, I.Y.Lee, L.G.Moretto, J.O.Newton, R.Schmitt, and F.S.Stephens, Phys. Rev. Lett. **38**, 331 (1977).

16. G.J.Mathews, G.J.Wozniak, R.P.Schmitt, and L.G.Moretto, Z. Phys. **A283**, 247 (1977).

17. P.Russo, R.P.Schmitt, G.J.Wozniak, R.C.Jared, P.Glässel, B.Cauvin, J.S.Sventek, and L.G.Moretto, Nucl. Phys. **A281**, 509 (1977).

18. W.Nörenberg, Phys. Lett. **53B**, 289 (1974).

19. L.G.Moretto and J.S.Sventek, Phys. Letters **58B**, 26 (1975).

20. L.G.Moretto, R.P.Babinet, J.Galin, and S.G.Thompson, Phys. Lett. 58B, 31 (1975).

21. J.Randrup, NORDITA preprint 77-45 (1977), to be published.

22. J.Blocki, J.Randrup, W.J.Swiatecki, and C.F.Tsang, Ann. Phys. 105, 427 (1977).

23. L.G.Moretto, J. Phys. Soc. Japan 44, Suppl. 7, 369 (1978).

24. J.S.Sventek and L.G.Moretto, Phys. Rev. Letters 40, 697 (1978).

25. J.R.Huizenga, J.R.Birkelund, W.U.Schröder, K.L.Wolf, and V.E. Viola, Phys. Rev. Letters 37, 885 (1976).

26. M.M.Aleonard, G.J.Wozniak, P.Glässel, M.M.Deleplanque, R.M.Diamond, L.G.Moretto, R.P.Schmitt, and F.S.Stephens, Phys. Rev. Lett. 40, 622 (1978).

27. P.Christensen, F.Folkmann, O.Hansen, O.Nathan, N.Trautner, F.Videbaek, S.Y.van der Werf, H.C.Britt, R.P.Chestnut, H.Freiesleben, and F.Pühlhofer, Phys. Rev. Letters 40, 1245 (1978).

28. R.Regimbart, A.N.Behkami, G.J.Wozniak, R.P.Schmitt, J.S.Sventek, and L.G.Moretto, submitted to Phys. Rev. Letters.

29. R.S.Simon, M.V.Banaschik, R.M.Diamond, J.O.Newton, and F.S. Stephens, Nucl. Phys. A290, 253 (1977).

30. P.Russo, R.P.Schmitt, G.J.Wozniak, B.Cauvin, P.Glassel, R.C.Jared, and L.G.Moretto, Phys. Letters 67B, 155 (1977).

31. G.J.Wozniak, R.P.Schmitt, P.Glässel, R.C.Jared, G.Bizard, and L.G.Moretto, Phys. Rev. Letters 40, 1436 (1978).

32. R.C.Jared, P.Glässel, J.B.Hunter, and L.G.Moretto, NIM (in press, 1977).

33. P.Dyer, R.J.Puigh, R.Vandenbosch, T.D.Thomas, and M.S.Zisman, Phys. Rev. Letters. 39, 392 (1977).

34. S.R.DeGroot and H.A.Tolhoek, Beta- and Gamma-Ray Spectroscopy, edited by K.Siegbahn (North-Holland, Amsterdam, 1955), p.616.

35. M.Berlanger, M.A.Deleplanque, C.Gerschel, F.Hanappe, M.LeBlanc, J.F.Mayault, C.Ngô, D.Paya, N.Perrin, J.Péter, B.Tamain, and -.Valentin, J. de Phys. Letters 37, L323 (1976).

36. J.B.Natowitz, M.M.Namboodiri, P.Kasiraj, R.Eggers, L.Adler, P.Gonthier, C.Cerruti, and T.Alleman, Phys. Rev. Lett. 40, 751 (1978).

37. L.G.Moretto, J.S.Sventek, and G.Mantzouranis, Lawrence Berkeley Laboratory Reprot LBL-7732 (1978), submitted to Phys. Rev. Letters.

38. A.Bohr and B.R.Mottelson, Nuclear Structure, Vol. II (W. H. Benjamin, Inc., Reading, Massachusetts, 1975).

39. C.Bloch, Nucl. Phys. $\underline{4}$, 503 (1957).

FIGURE CAPTIONS

Fig. 1. Contour map of the cross section for K ions in the $E_{c.m.}$ - $\theta_{c.m.}$ plane for the reaction ^{232}Th + 388 MeV ^{40}Ar.

Fig. 2. Contour plots of the cross section in the total kinetic energy-angle plane for various exit channel asymmetries in the reaction 620 MeV ^{86}Kr + ^{197}Au.

Fig. 3. Mean center of mass fragment kinetic energies and widths as a function of fragment Z.

Fig. 4. Masses prior to evaporation and number of evaporated neutrons versus the Z before evaporation. Symbols Δ and • refer to the light and heavy fragments, respectively.

Fig. 5. a) Missing charge versus total exit channel kinetic energy for various bombarding energies in the reaction ^{20}Ne + ^{63}Cu.
b) Missing charge versus excitation energy.

Fig. 6. Contour plots of $d^2\sigma/dE\,d\theta$ (arbitrary units) in the E_{lab}, mass plane for the K isotopes detected at θ_{lab} = 18° (close to the θ_{graz}) and θ_{lab} = 8°.

Fig. 7. Gamma-multiplicity as a function of Z for the ^{nat}Ag + 175 MeV ^{20}Ne reaction at three lab angles.

Fig. 8. a) Lab charge distributions for the reaction ^{197}Au + 506 MeV ^{86}Kr. b) Lab charge distributions for the reaction ^{nat}Ag + 732 MeV ^{86}Kr.

Fig. 9. Potential energies versus the atomic number of one fragment for various angular momenta for the system ^{86}Kr + ^{197}Au.

Fig. 10. Diffusion calculations for the system 620 MeV ^{86}Kr + ^{197}Au for the same ℓ waves as in Fig. 9.

Fig. 11. Z distributions calculated from the diffusion model for ^{197}Au and ^{181}Ta + 620 MeV ^{86}Kr. The dots are the experimental results.

Fig. 12. Angular distributions for fragments of different atomic number for the reactions ^{197}Au and ^{181}Ta + 620 MeV ^{86}Kr. The solid lines represent the theoretical results.

Fig. 13. a) Lines of constant total angular momentum in the Z, TKE plane without angular momentum transfer; b) Same as in a) for a rigidly rotating system; c) Qualitative expectations for the correct lines of constant angular momentum.

Fig. 14. a) Lines of constant angular momentum in the TKE versus Z plane. b) An expanded view of a) including contours of constant cross section.

Fig. 15. The ratio of the charge widths calculated for energy cuts along lines of constant angular momentum and of constant total kinetic energy versus the bin number for the energy loss.

Fig. 16. M_γ versus total kinetic energy for three ^{86}Kr-induced reactions. The data have been averaged over ten Z-values. The solid and dashed curves are fits to the data.

Fig. 17. Gamma-ray multiplicities versus Z for the quasi-elastic component in 618 MeV ^{86}Kr + ^{165}Go and ^{197}Au.

Fig. 18. Gamma-ray multiplicities versus Z for the deep-inelastic component in 618 MeV ^{86}Kr + ^{107,109}Ag, ^{165}Ho and ^{197}Au.

Fig. 19. M_γ versus Z_3 for the reactions ^{107,109}Ag and ^{165}Ho + 618 MeV ^{86}Kr for the quasi-elastic (open symbols) and deep-inelastic (solid symbols) components. Solid curves are fits to the data.

Fig. 20.   (Top): Cross section contour lines in the E_4-Z_3 plane for coincident events. (Bottom): Percent fission of heavy recoils (Z_4 = 115-Z_3) integrated over the deep-inelastic component.

Fig. 21.   Percent fission of heavy recoils as a function of the lab energy of the light fragment.

Fig. 22.   FWHM of the out-of-plane fission and non-fission components as a function of Z_3.

Fig. 23.   The quantal curve (curve 1) and classical (curve 2) widths of the Z-distribution for fixed mass asymmetry versus excitation energy. Curve 3 is the sum of both contributions and the triangle indicates the experimental value.
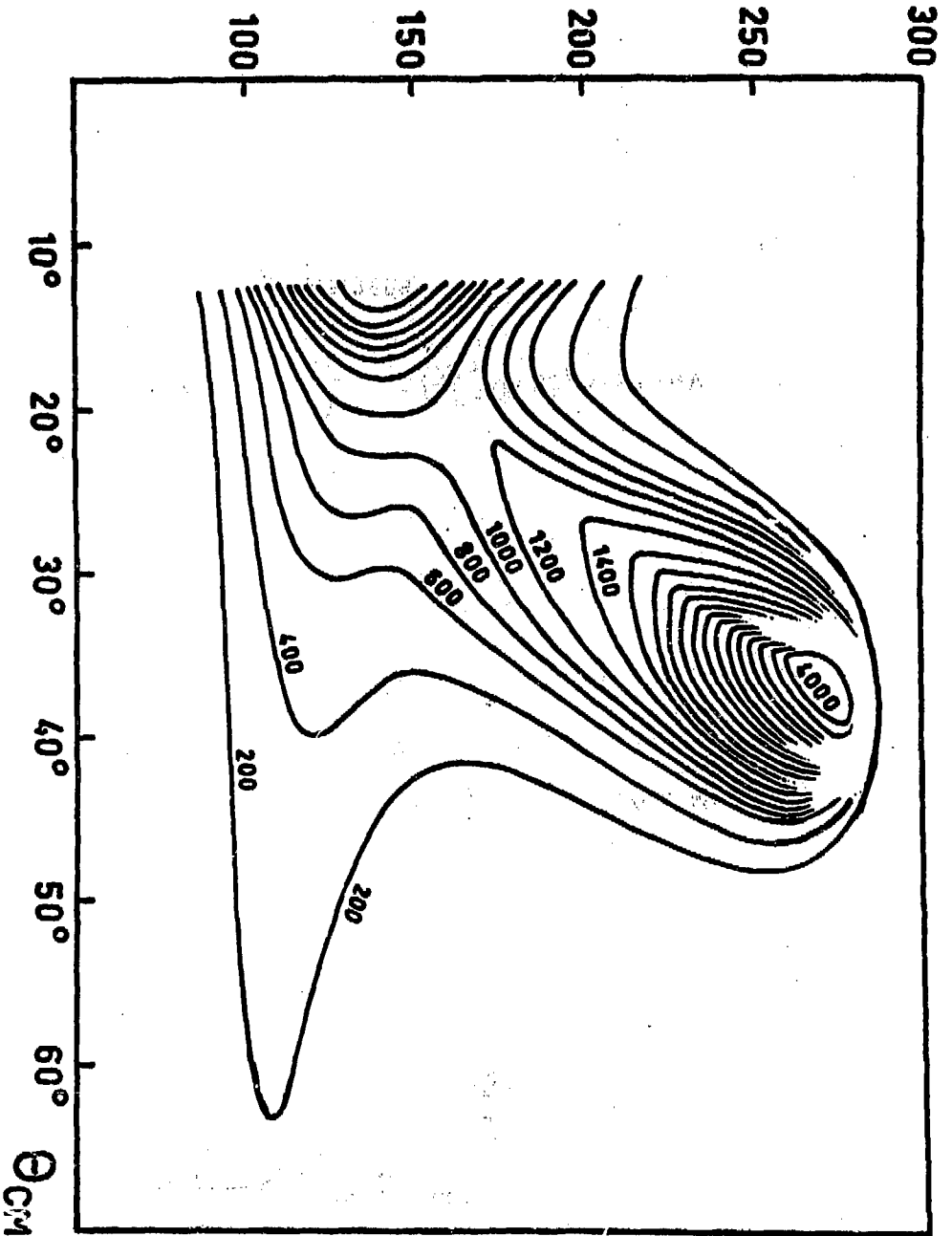
Figure 1

XBL 746-963

620 MeV ^{86}Kr + ^{197}Au
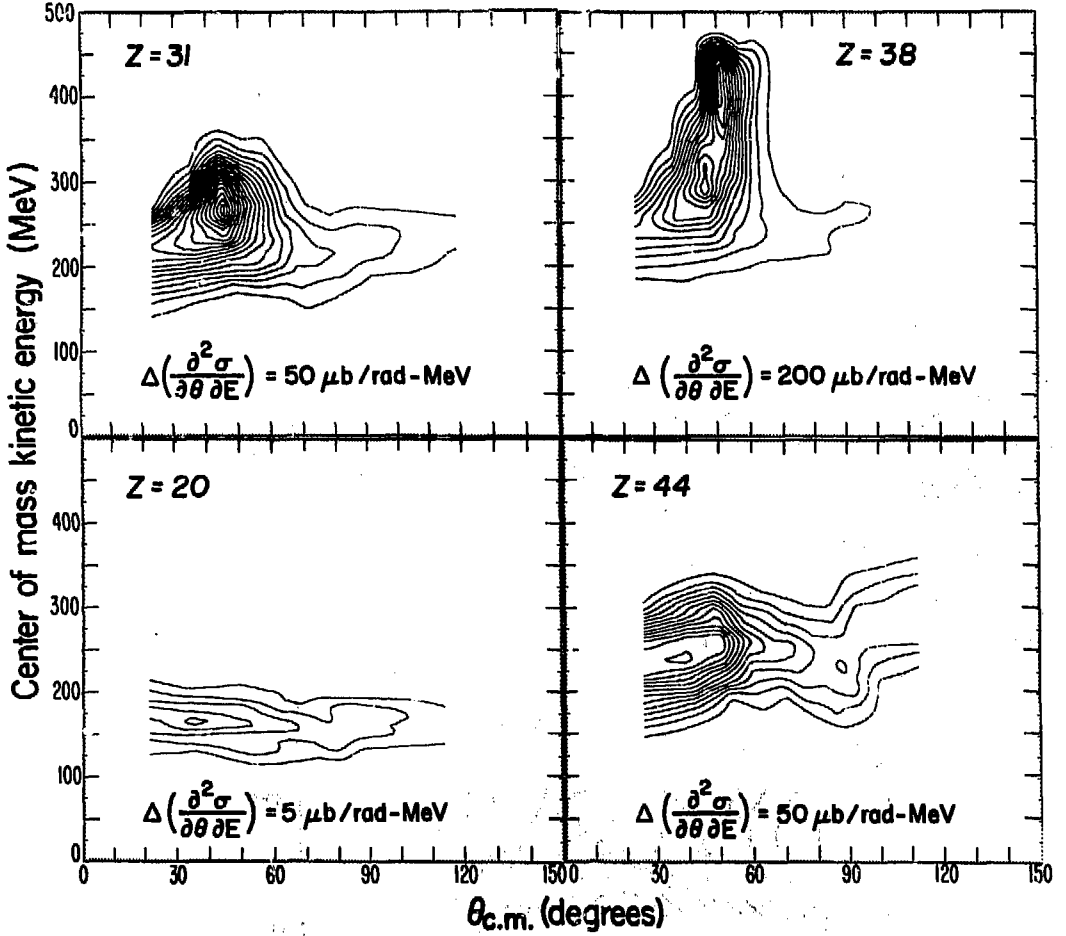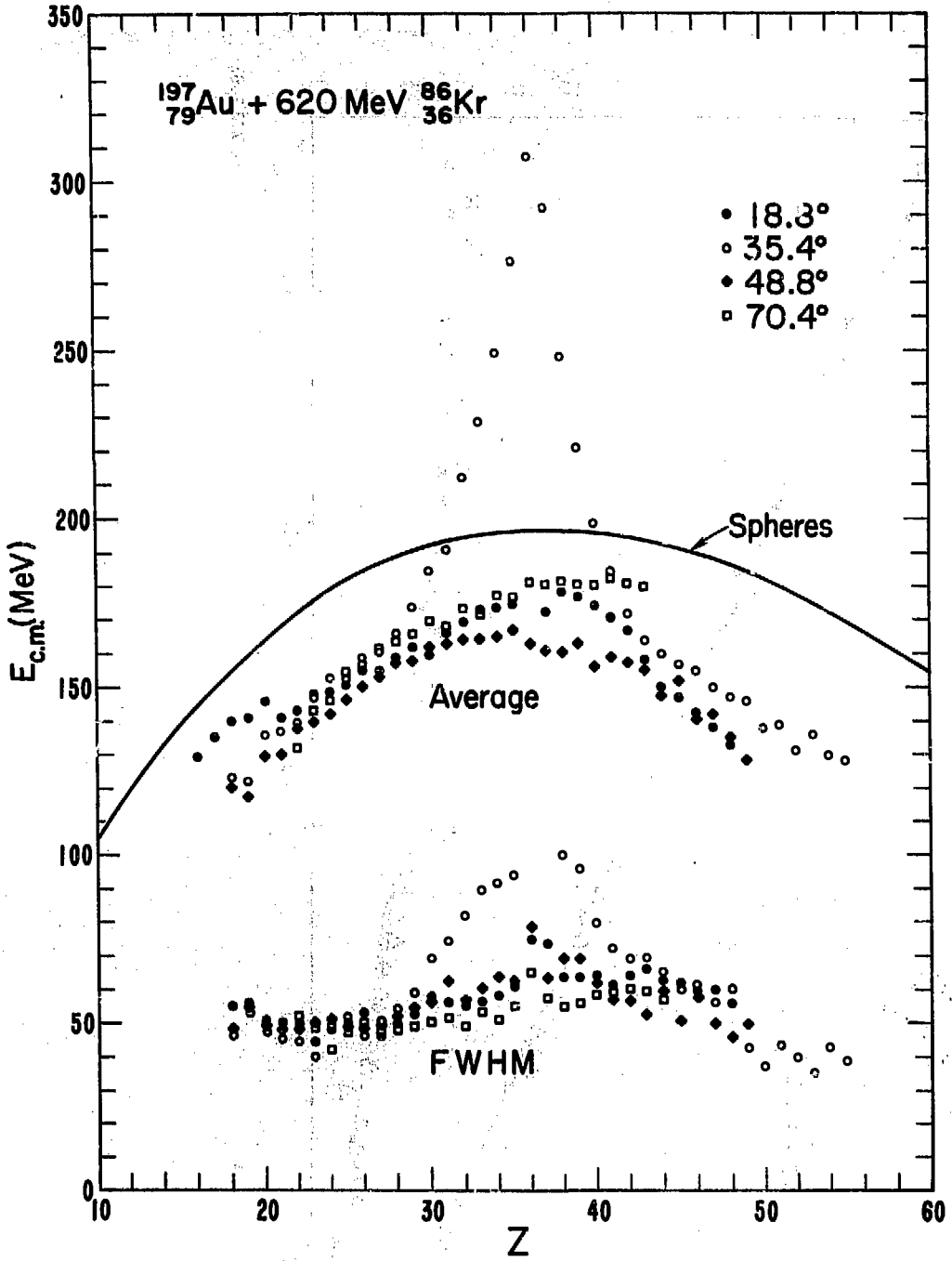
Figure 2

Figure 3

Figure 4

XBL 778-2563

Figure 5

Figure 6

XBL 788-9931

175 MeV ^{20}Ne + $^{nat.}$Ag
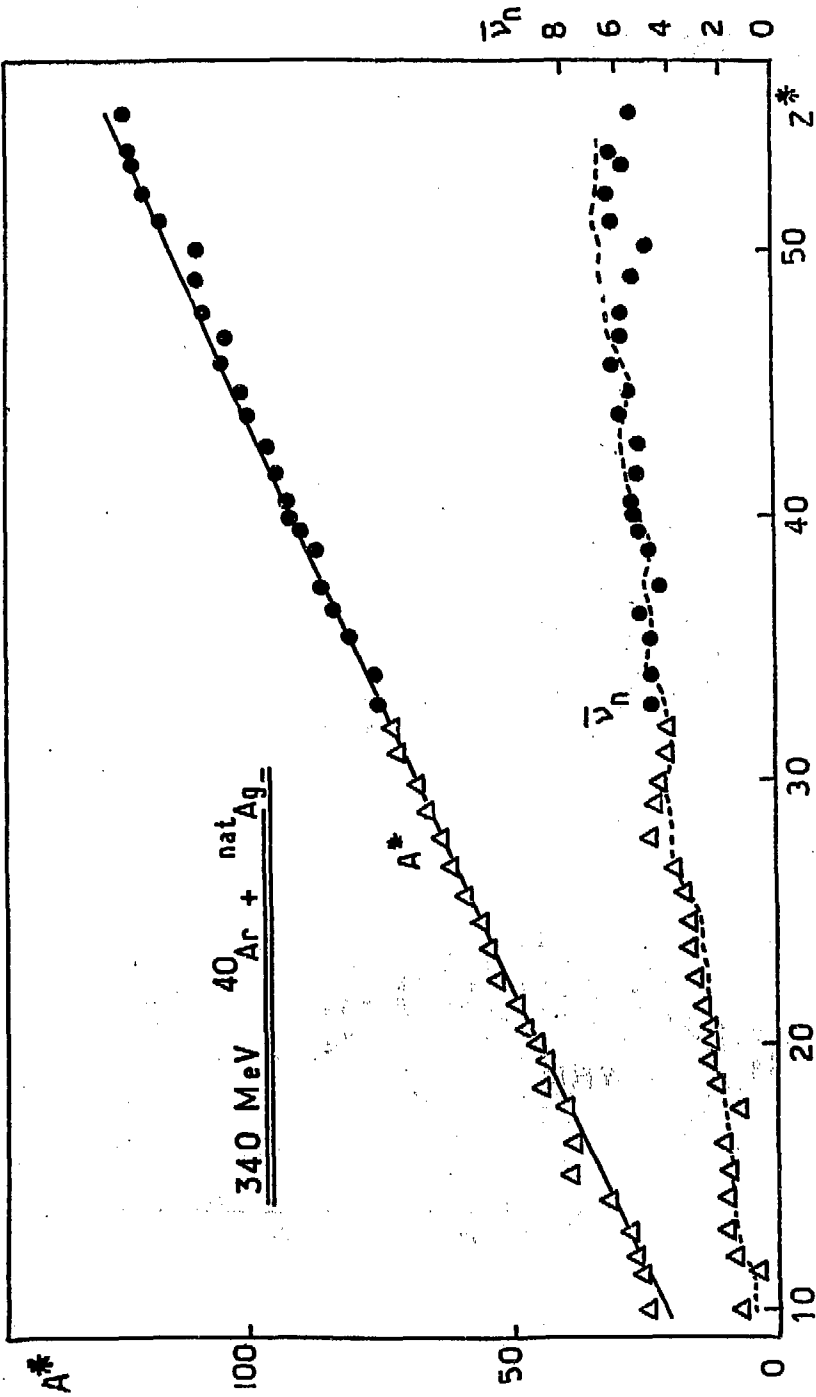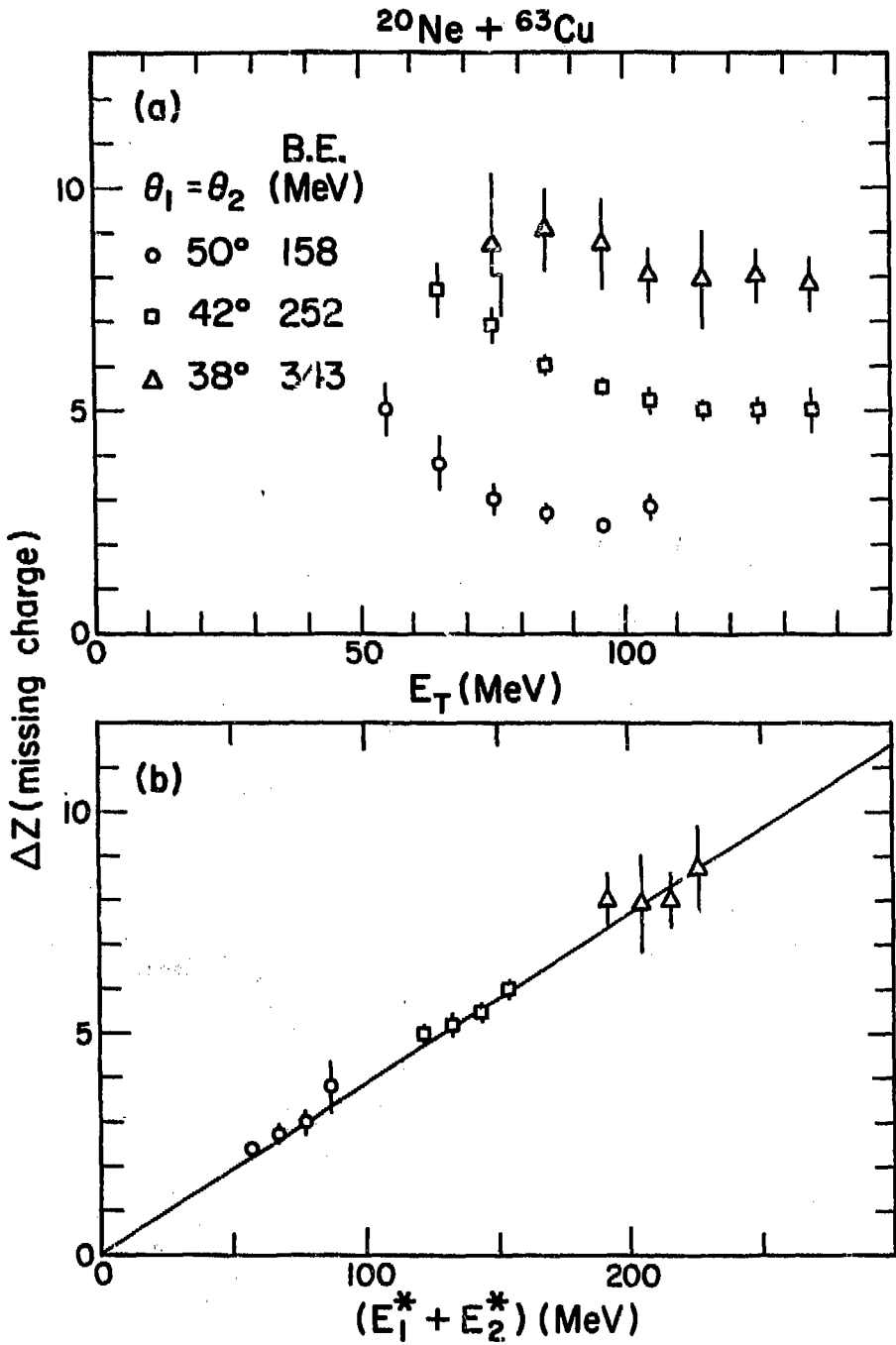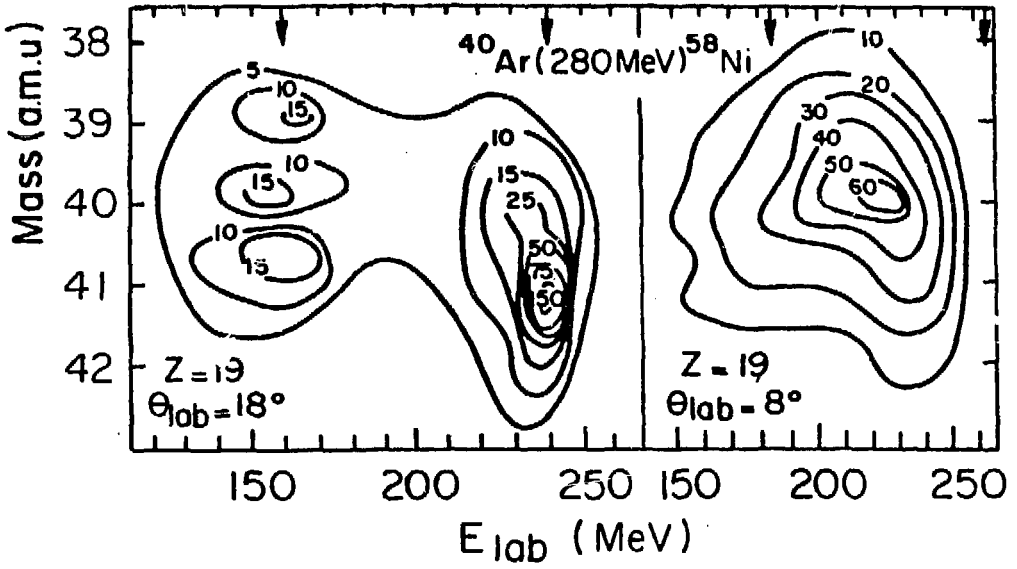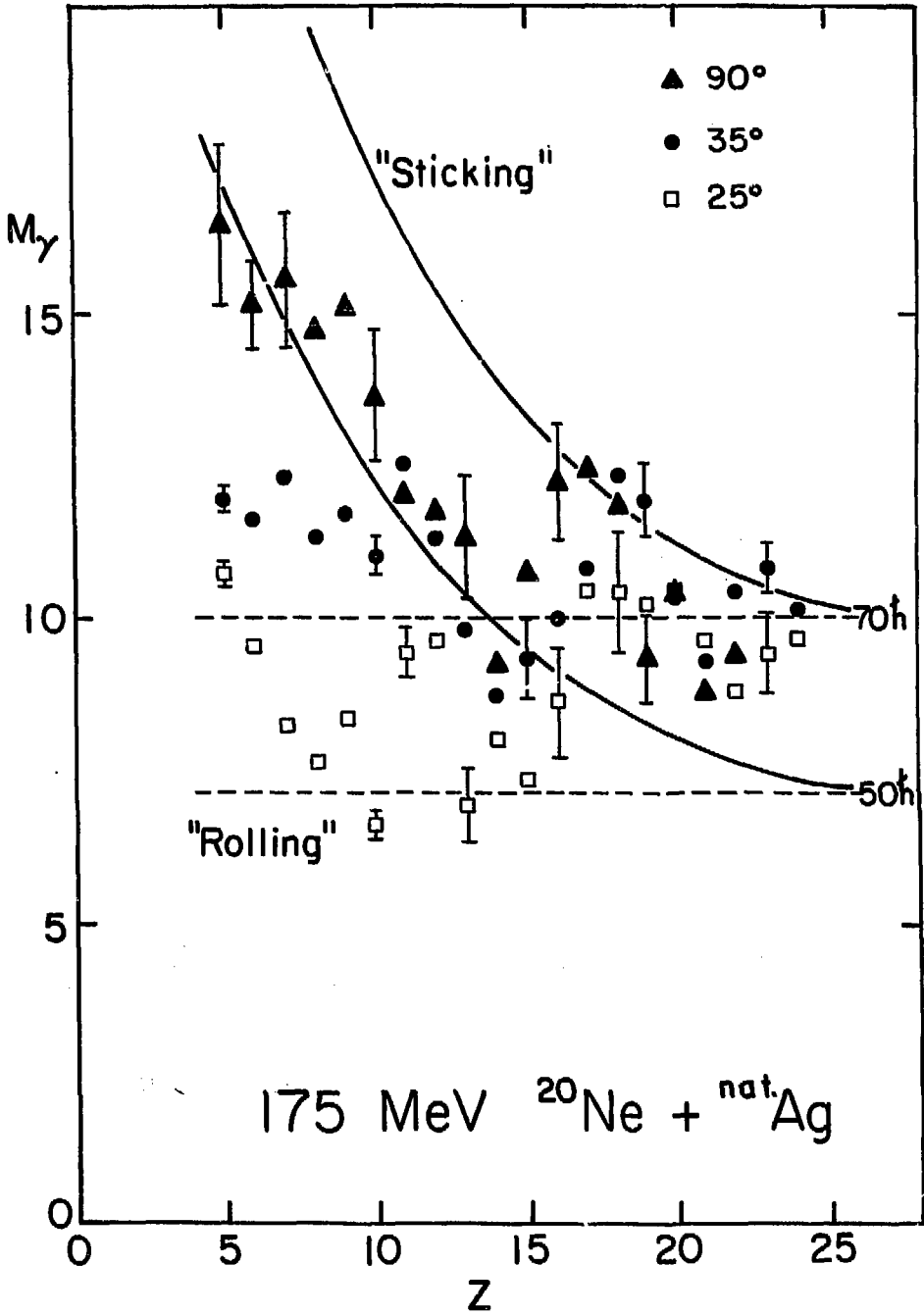
XBL 7611-4446

Figure 7
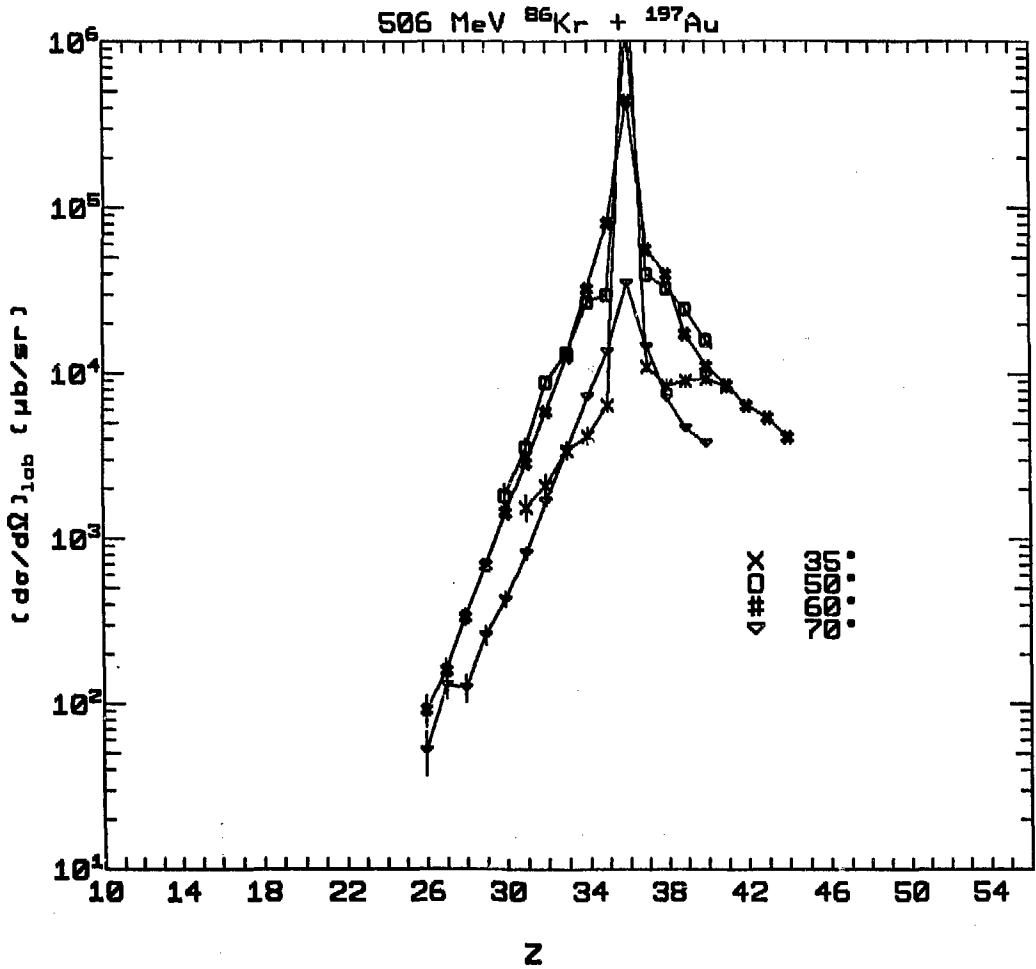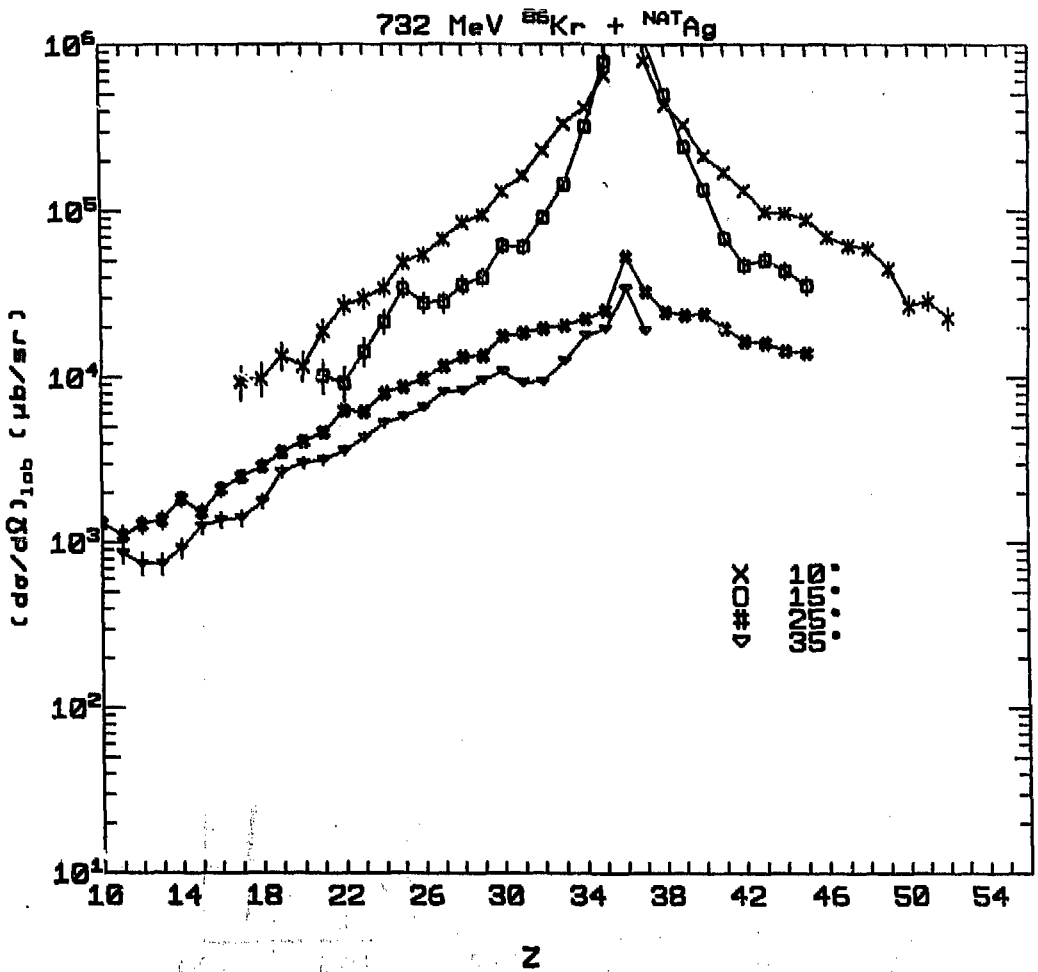
Figure 8a

Figure 8 b

620MeV ^{86}Kr + ^{197}Au
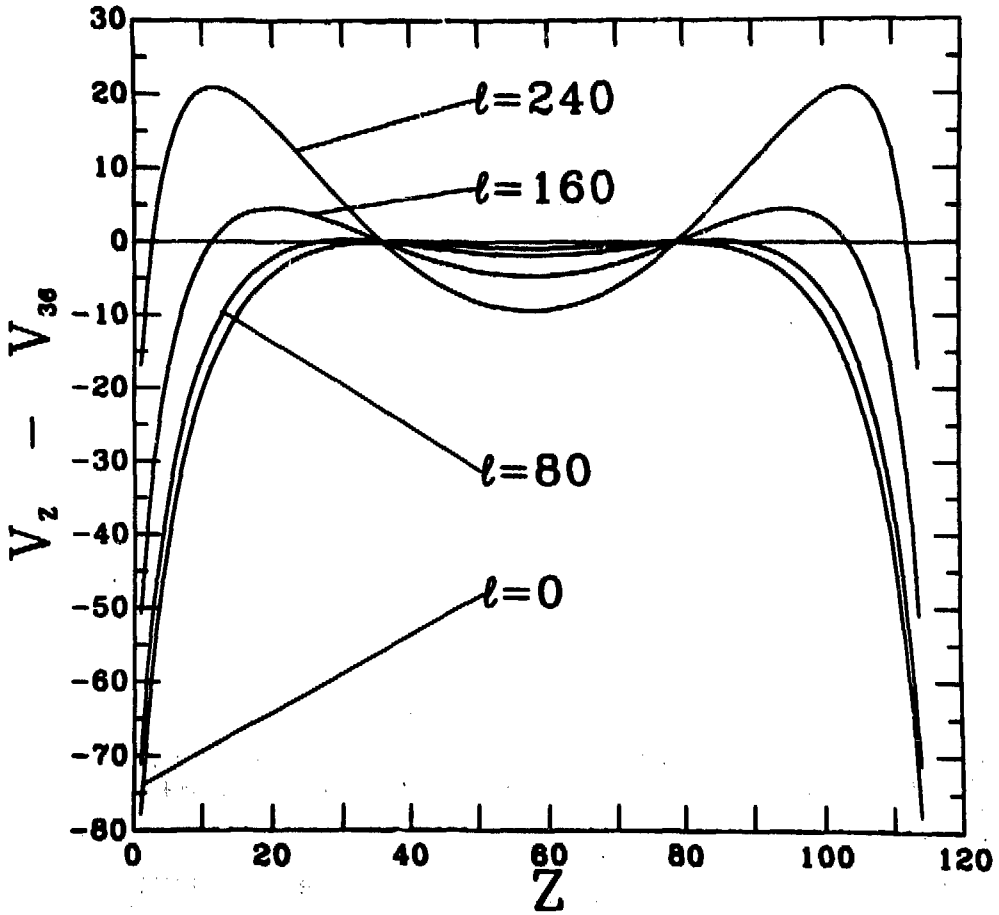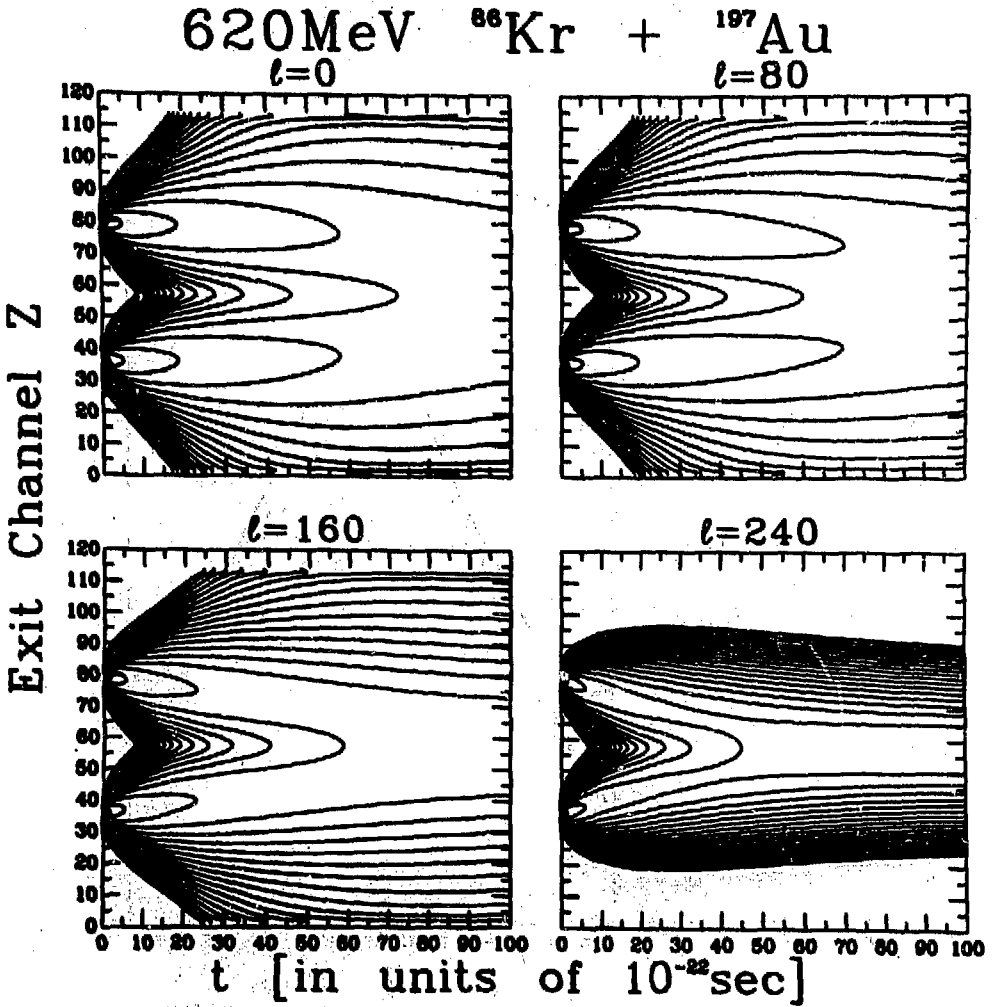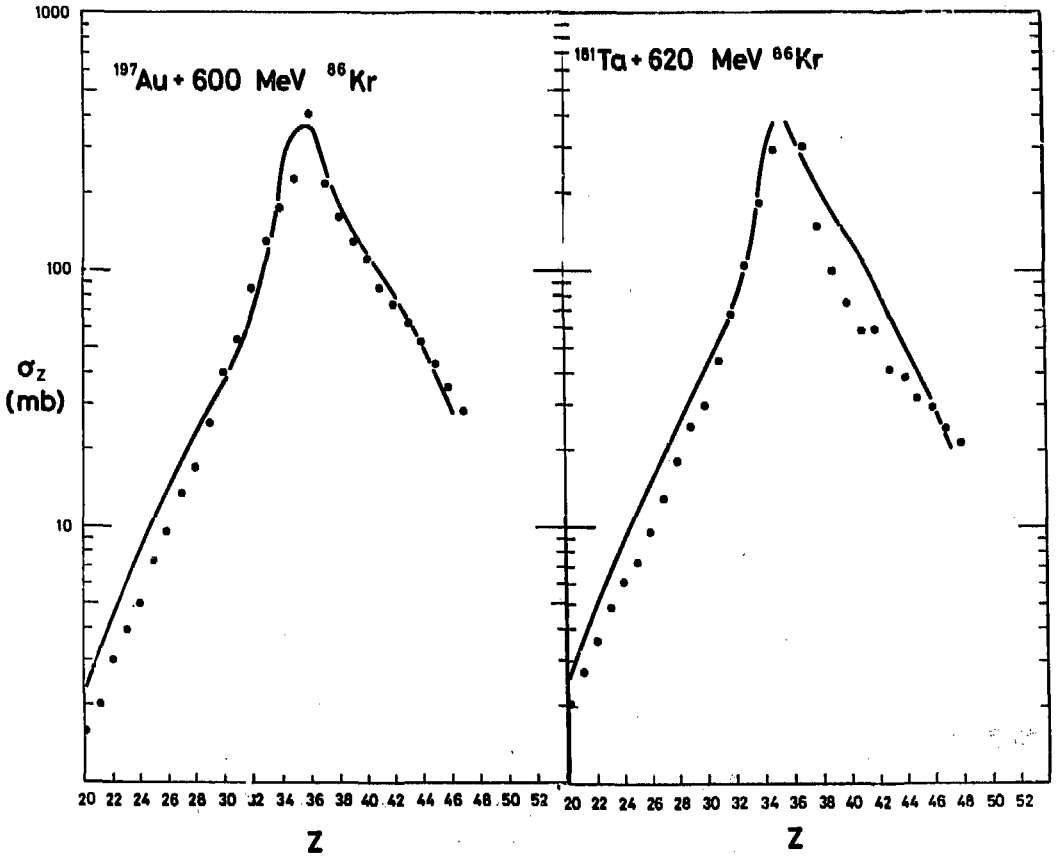
Figure 9

Figure 10

Figure 11

Figure 12

TKE

(a)

(b)

(c)

TKE

Z

XBL7711-10426

Figure 13

1156MeV ^{136}Xe + ^{197}Au

Figure 14

XBL7711-10427

Figure 15

618 MeV ^{86}Kr
Z = 30-39

^{107,109}Ag

^{165}Ho

^{197}Au

$\langle M_\gamma \rangle$

TKE (MeV)
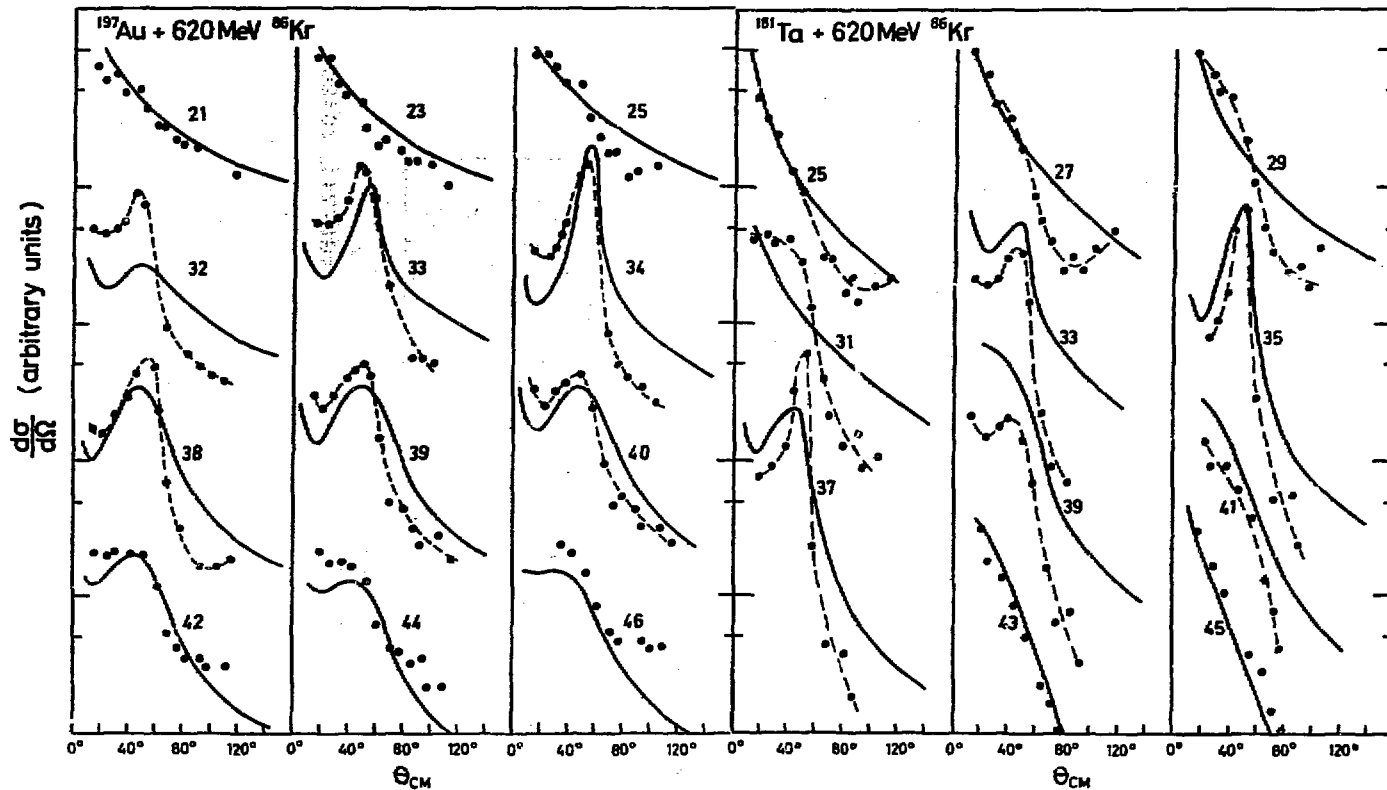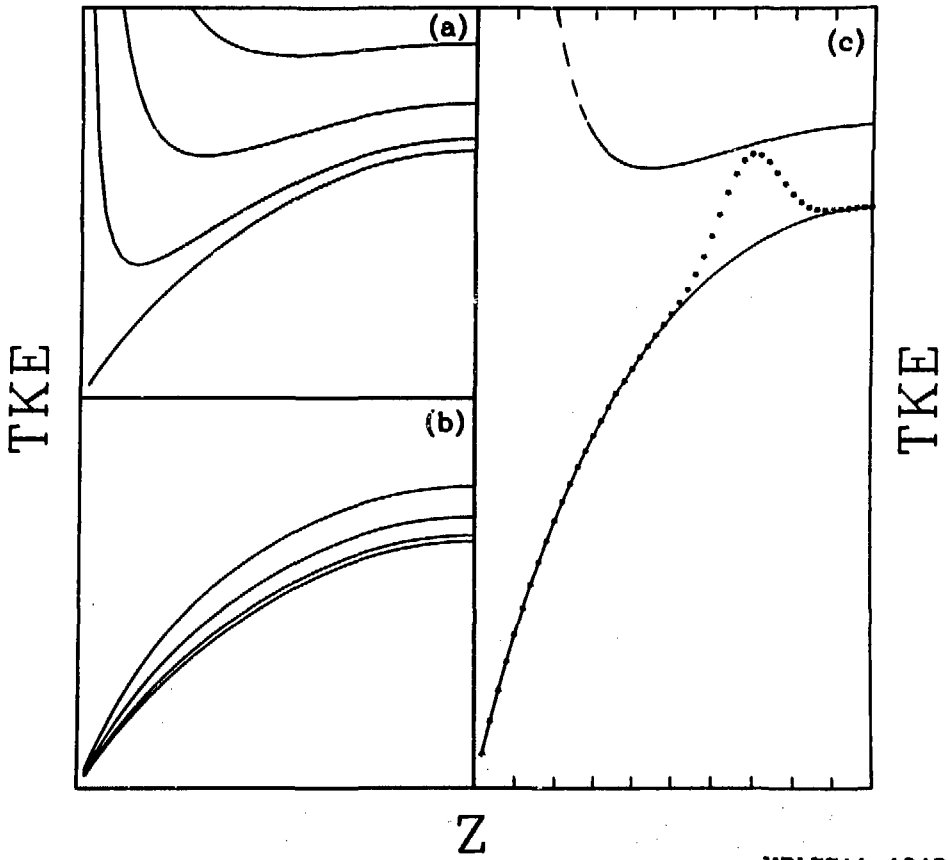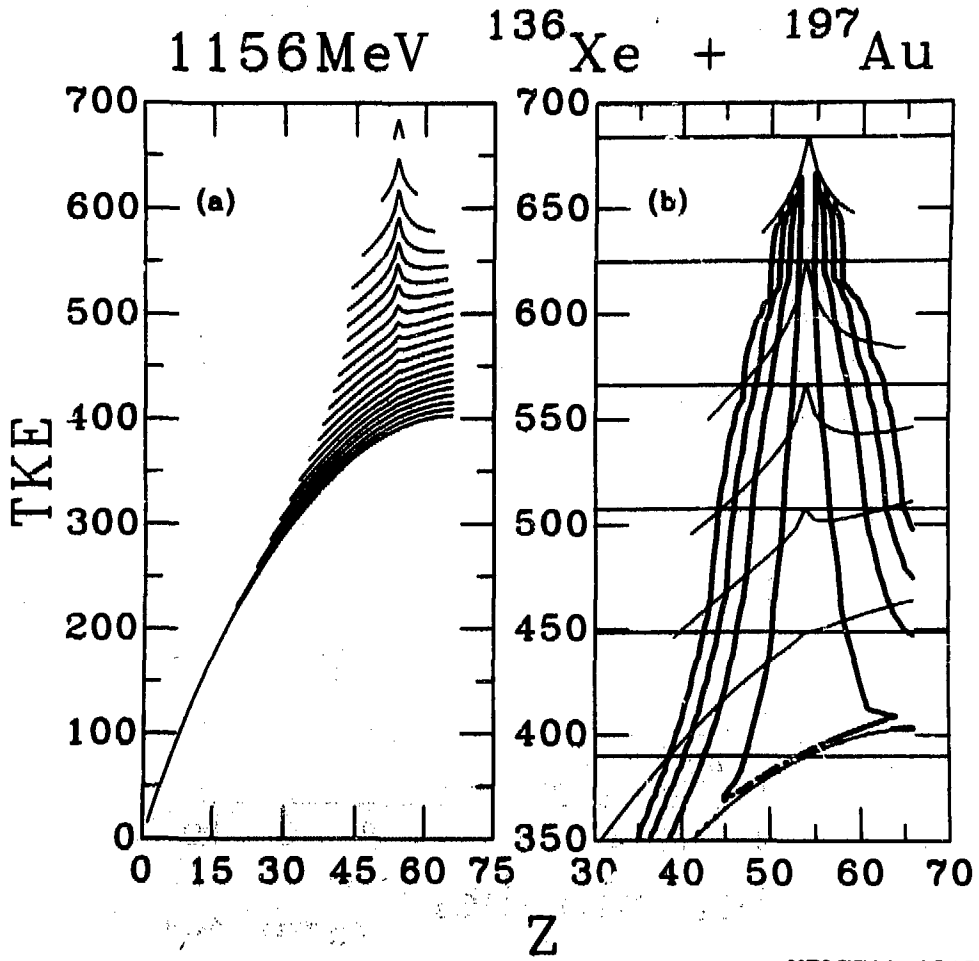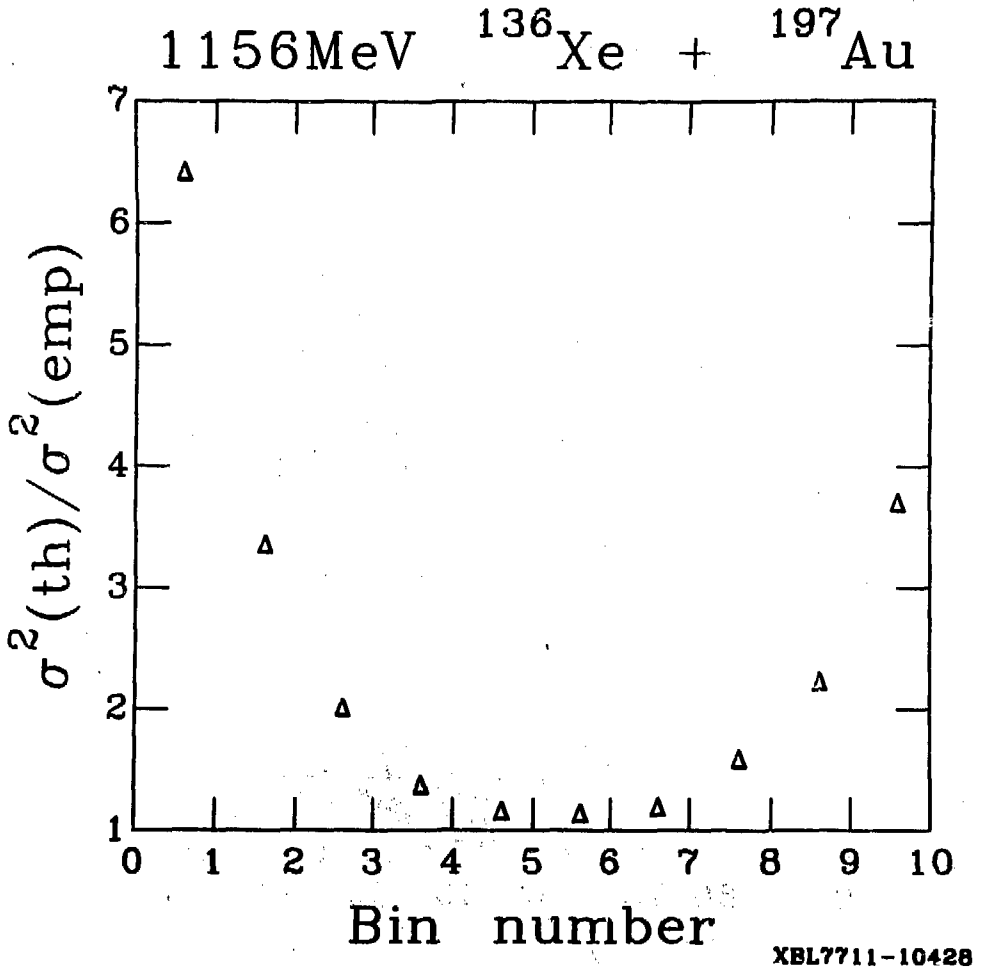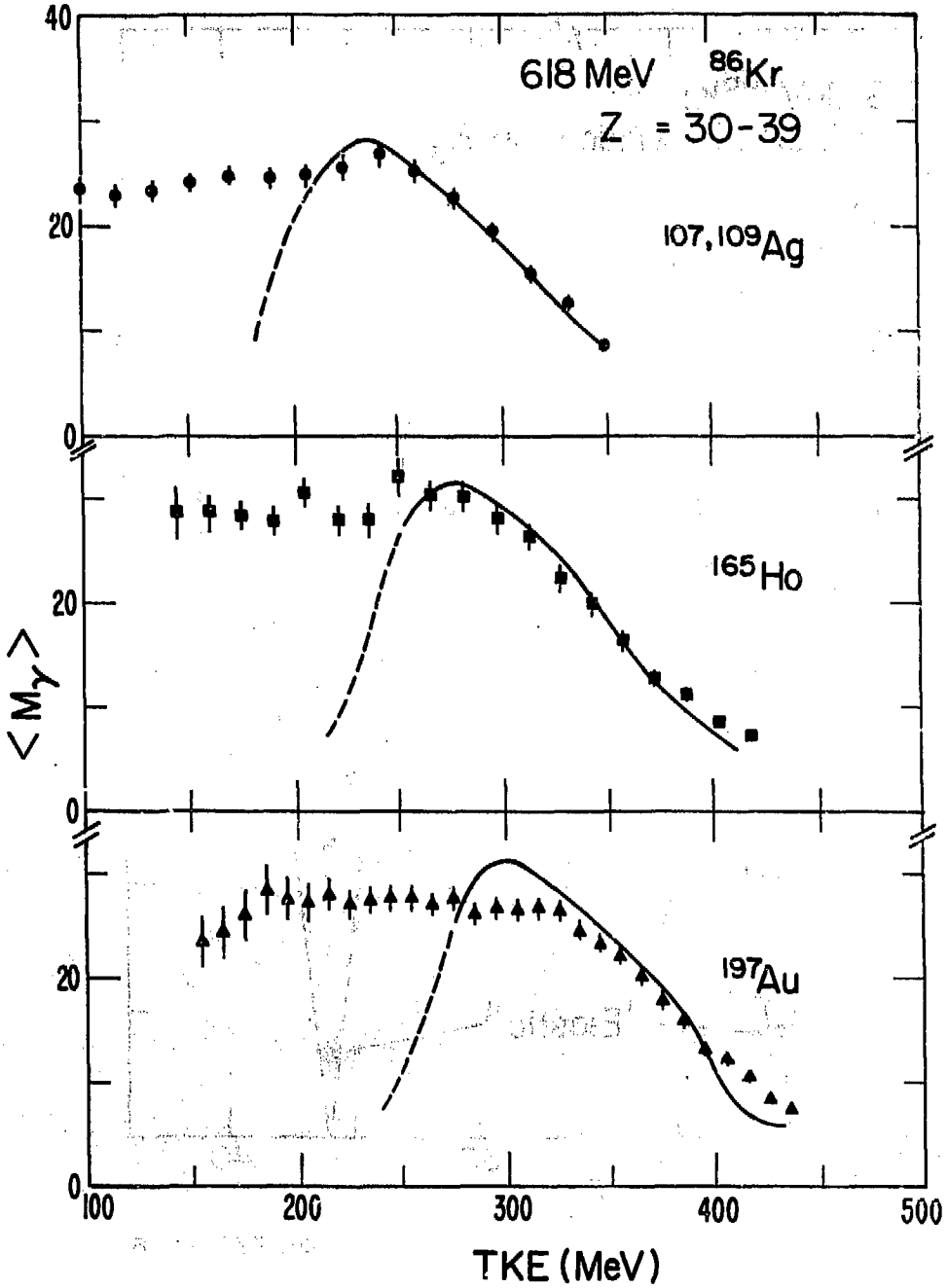
XBL 786-2553

Figure 16
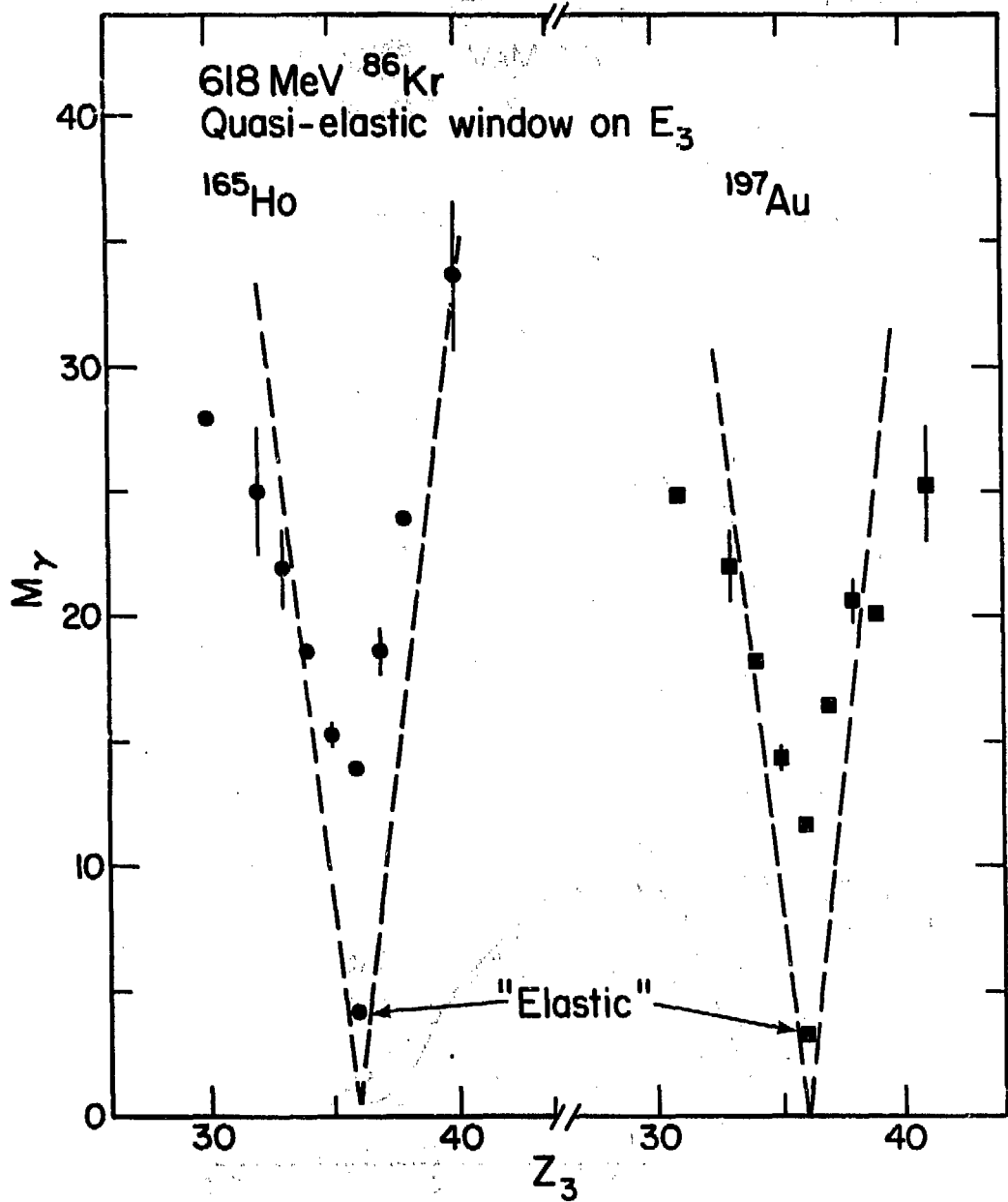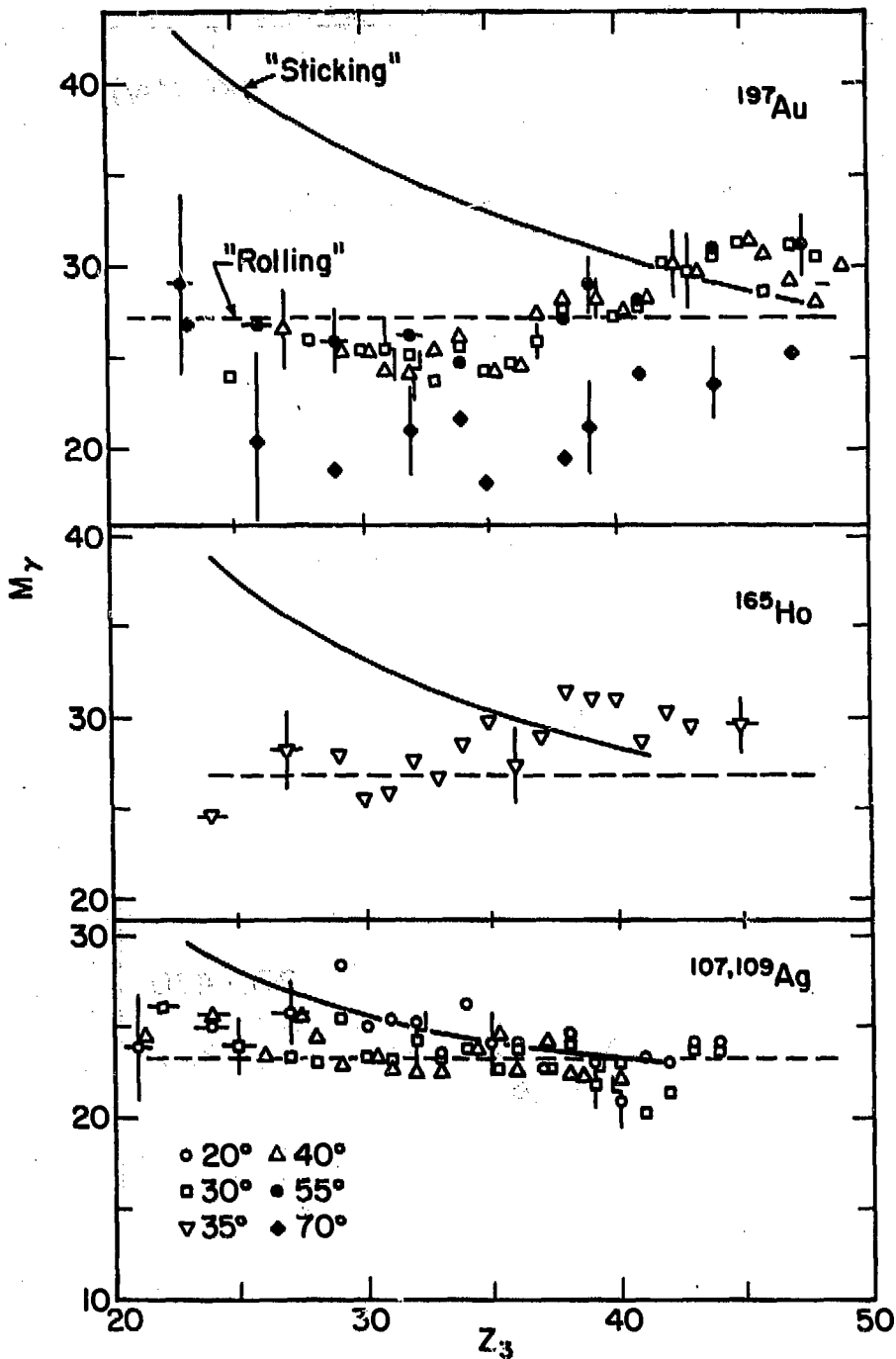
Figure 17

Figure 18

XBL 786-2556

Figure 19

Figure 20

618 MeV ^{86}Kr + ^{197}Au

Fissionability of $Z_4 = 115 - Z_3$

E_3 (MeV)

$Z_3 = 30$

$Z_3 = 34$

$Z_3 = 32$

$Z_3 = 36$
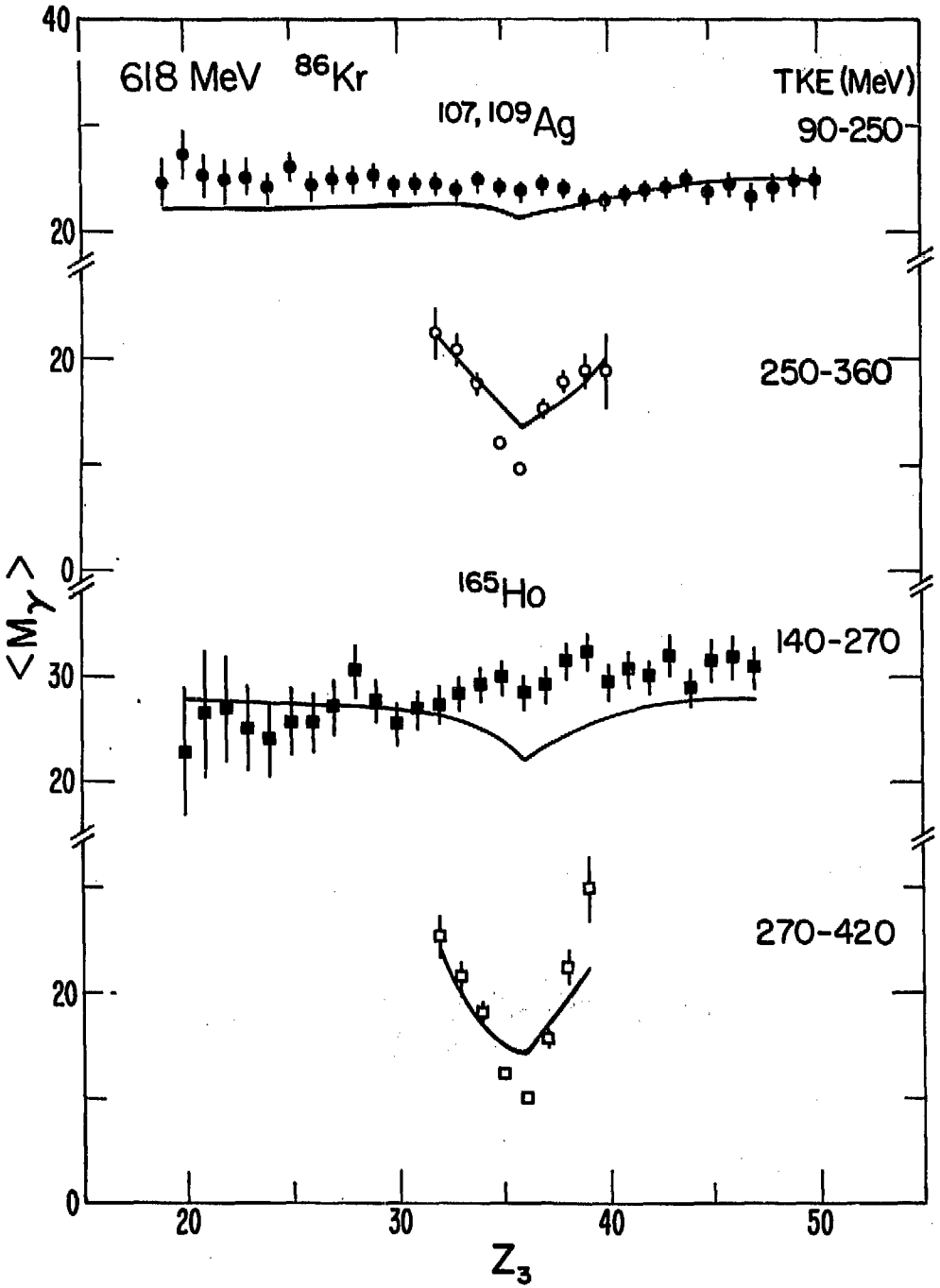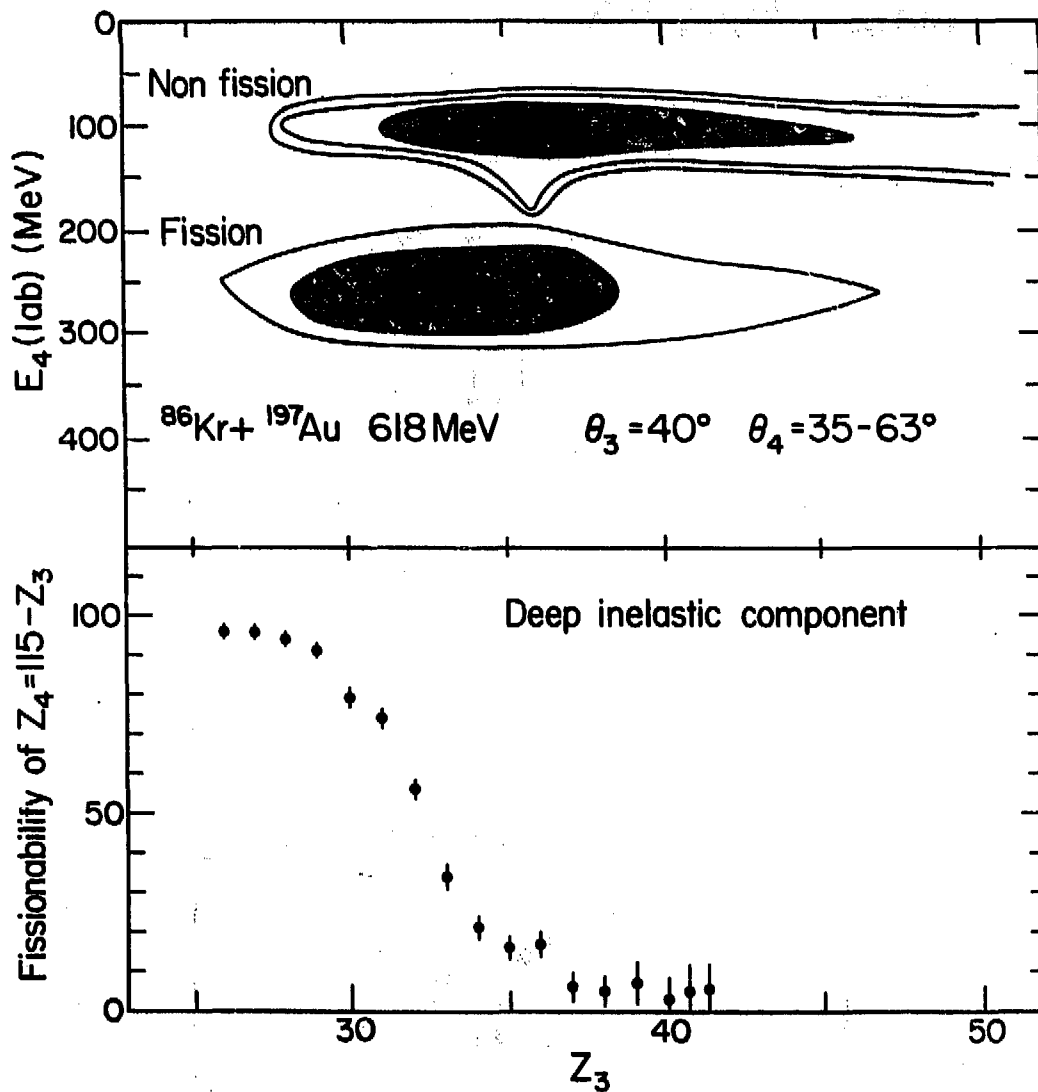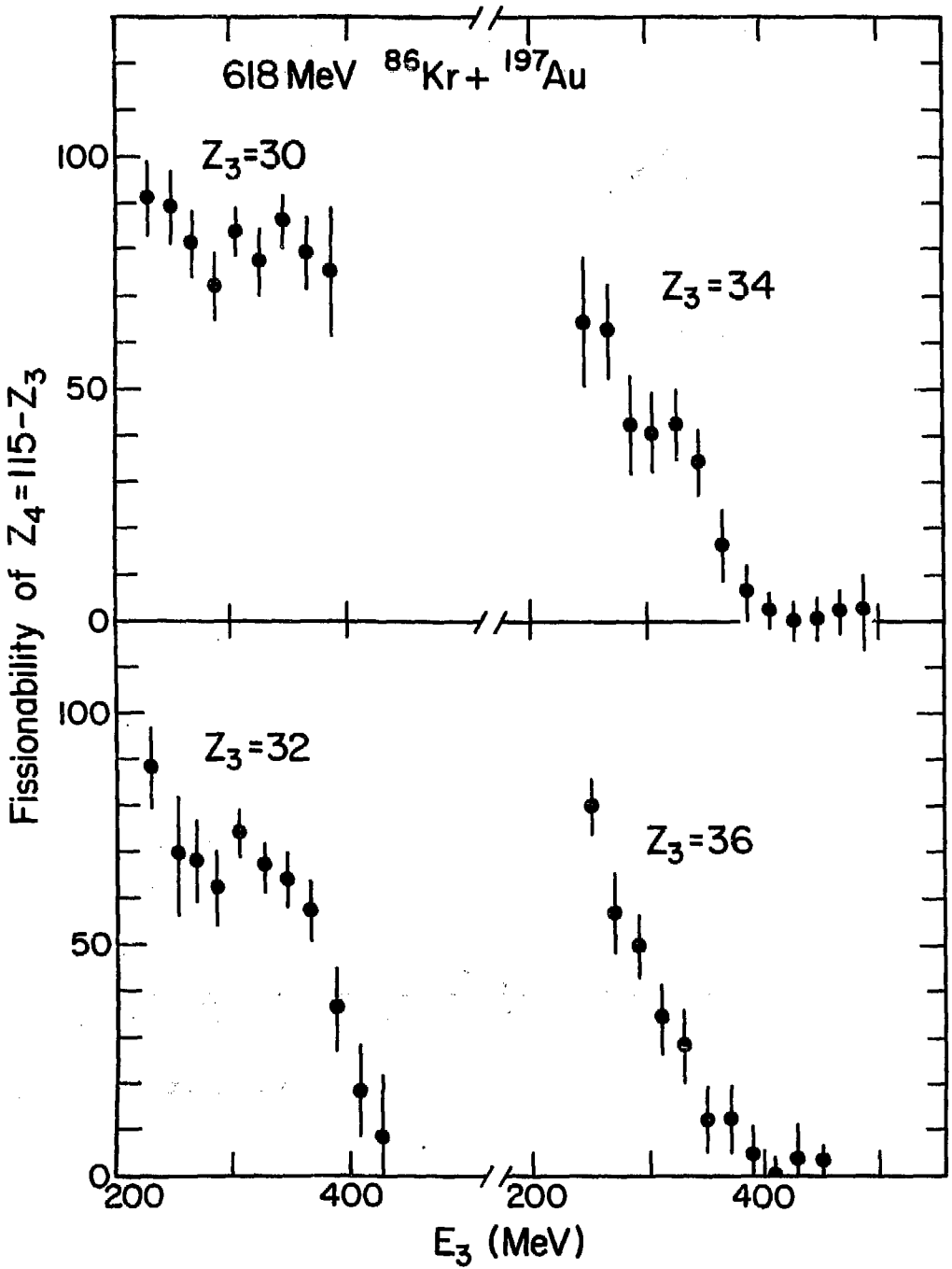
XBL 7712-11080

Figure 21

Figure 22

Figure 23